

# Federated Learning for Energy-limited Wireless Networks: A Partial Model Aggregation Approach

Zhixiong Chen, *Student Member, IEEE*, Wenqiang Yi, *Member, IEEE*, Arumugam Nallanathan, *Fellow, IEEE*, and Geoffrey Ye Li, *Fellow, IEEE*

## Abstract

The limited communication resources, e.g., bandwidth and energy, and data heterogeneity across devices are two of the main bottlenecks for federated learning (FL). To tackle these challenges, we first devise a novel FL framework with partial model aggregation (PMA), which only aggregates the lower layers of neural networks responsible for feature extraction while the upper layers corresponding to complex pattern recognition remain at devices for personalization. The proposed PMA-FL is able to address the data heterogeneity and reduce the transmitted information in wireless channels. We then obtain a convergence bound of the framework under a non-convex loss function setting. With the aid of this bound, we define a new objective function, named the scheduled data sample volume, to transfer the original inexplicit optimization problem into a tractable one for device scheduling, bandwidth allocation, computation and communication time division. Our analysis reveals that the optimal time division is achieved when the communication and computation parts of PMA-FL have the same power. We also develop a bisection method to solve the optimal bandwidth allocation policy and use the set expansion algorithm to address the optimal device scheduling. Compared with the state-of-the-art benchmarks, the proposed PMA-FL improves 2.72% and 11.6% accuracy on two typical heterogeneous datasets, i.e., MNIST and CIFAR-10, respectively. In addition, the proposed joint dynamic device scheduling and resource optimization approach achieve slightly higher accuracy than the considered benchmarks, but they provide a satisfactory energy and time reduction: 29% energy or 20% time reduction on the MNIST; and 25% energy or 12.5% time reduction on the CIFAR-10.

## Index Terms

Device scheduling, federated Learning, Lyapunov optimization, resource management

Zhixiong Chen, Wenqiang Yi, and Arumugam Nallanathan are with the School of Electronic Engineering and Computer Science, Queen Mary University of London, London, U.K. (emails: {zhixiong.chen, w.yi, a.nallanathan}@qmul.ac.uk).

Geoffrey Ye Li is with the Faculty of Engineering, Department of Electrical and Electronic Engineering, Imperial College London, England (e-mail: geoffrey.li@imperial.ac.uk).

Part of this work was submitted in IEEE Global Communications Conference (GLOBECOM), December, Brazil, 2022 [1].

## I. INTRODUCTION

Federated learning (FL) is a promising distributed learning approach for protecting data privacy. In FL, edge devices collaboratively train a model under the orchestration of a parameter server (PS), which only requires local learning models/gradients instead of local private data [2]. FL operations can be divided into two parts, namely the communication part and the computation part [3]. For the communication part, the learning performance is constrained by the limited communication resources, e.g., bandwidth and energy. For the computation part, the model accuracy is degraded by non-independent and identically distributed (non-IID) data samples. More specifically, the inadequate wireless resources hinder more devices devoted to the FL training process, and thus negatively affect the convergence speed and learning accuracy [4], [5]. Moreover, since the PS aggregates models learned from the different devices, the data heterogeneity presented on different devices may lead to weak generalization ability of the trained global model, even resulting in an unstable training process of FL [6]. Therefore, FL needs well-designed solutions to address these two challenges.

### A. Related Works and Motivations

From the communication perspective, efficient resource management and scheduling schemes can enable additional devices to participate in the FL process and thus enhancing learning performance. To this end, existing works focus on resource optimization [7]–[9], device selection [10]–[14], and alternating direction method of multipliers to reduce the communication rounds of training [15]. The energy-efficient workload partitioning scheme in [7] balances the computation between the central processing unit and graphics processing unit in the FL system. The time-sharing based transmission scheme in [8] can improve the communication efficiency of FL. Using this time-sharing scheme, a device heterogeneity-aware scheduling scheme has been proposed in [9] to maximize the number of scheduled data samples under energy constraint. The joint device scheduling and resource allocation policy in [10] maximizes the model accuracy in latency constrained FL. The joint client selection and bandwidth allocation scheme in [11] maximizes the scheduled data samples under long-term client energy constraints. In [12], a gradient norm approximation method can assist device schedule for boosting the training performance in the over-the-air FL system. The importance and channel-aware device scheduling policy in [13] accelerates the convergence of FL. A joint learning, wireless resource allocation, and user selection problem has been investigated in [14] to minimize an FL loss function. Although these

works have devised different device scheduling and resource management policies to facilitate FL, the joint optimization of communication and computation in FL has been rarely explored.

From the computation perspective, the emerging personalized FL techniques are promising to tackle the data heterogeneity related challenges, which adapts the collaboratively learned global model for individual clients. Most personalized federated learning techniques involve two steps: 1) devices train a global model in a collaborative fashion, 2) each device personalizes the global model using their private data. Existing works toward this direction utilize various techniques to implement model personalization in the latter step, including multi-task learning [16], meta-learning [17], model regularization [18], and model interpolation [6]. More specifically, it has been showed in [16] that multi-task learning is a natural choice to build personalized federated models. However, the multi-task FL heavily relies on the full participation of devices in each round. The model-agnostic meta-learning algorithm in [17] can improve the model accuracy of FL, which maps the meta-training to the federated training process and meta-testing to FL personalization. A proximal term is introduced in [18] to limit the impact of local updates, achieving convergence stability and improving model generalization. Based on this, parameter importance is further considered in [19] to regularize the local loss function. The adaptive personalized FL algorithm in [6] can find the optimal combination of global and local models in a communication efficient manner. However, the above techniques require more computation or memory resources than the conventional FL algorithms that solely train a global model, e.g., Federated Averaging (FedAvg) [20]. To reduce the training cost, the learning model in [21] is decoupled into two parts, i.e., body part and head part, proposed to learn a shared body part and unique local heads for clients, in which the body part and local heads are trained separately.

Based on the above discussion, an efficient FL approach should simultaneously tackle both the data heterogeneity across devices and communication resources limitations. Inspired by the success of centralized learning, different learning tasks often share the lower layers of neural networks responsible for feature extraction while the heterogeneity mainly focuses on the upper layers corresponding to complex pattern recognition [22], [23]. This work attempts to solve the following problems:

- **Problem 1:** How to joint optimize the device scheduling, communication and computation resource to maximize the learning performance of the FL under limited energy budgets and communication bandwidth of devices?
- **Problem 2:** How to design an more efficient FL algorithm than traditional FedAvg based

on feature extractor related layer sharing and theoretically demonstrate its convergence?

### *B. Contributions*

This work considers a typical federated supervised learning scenario, where a PS orchestrates multi-devices to enable the FL process. We aim to address both data heterogeneity and communication resources limitations. In particular, the FL process partially aggregates the model parameters of the devices to train a shared feature extractor. Different from [21], we simultaneously update the feature extractor and predictors in the local training phase and theoretically analyze the convergence bound of the proposed approach. The main contributions of this paper are summarized as follows:

- To tackle the data heterogeneity across devices in the FL system, we devise a novel federated learning framework, namely partial model aggregation-FL (PMA-FL), in which devices only collaboratively train the lower layers of the neural networks while the upper layers are individually trained by each device for personalization. This design can reduce the data volumes in the transmission phase and improve the model generalization on non-IID local datasets.
- To enable efficient FL in wireless networks, we minimize the global loss function while simultaneously considering devices' long-term energy budget, bandwidth limitation, and latency constraints. However, it is intractable to minimize the global loss due to its inexplicit form. To this end, we theoretically characterize the convergence bound of the considered FL system with the general non-convex loss function setting, finding a new metric, termed scheduled data sample volume, which is in an explicit form for the device scheduling policy. The minimum global loss function can be obtained by maximizing this metric.
- To maximize the scheduled data sample volume, we formulate a joint device scheduling, wireless bandwidth allocation, and computation-communication-time division optimization problem, which is a mixed-integer nonlinear programming problem and is challenging to solve. We first decouple the long-term stochastic problem into a deterministic one in each communication round with the assistance of the Lyapunov optimization framework. Then, we solve the one-shot optimization problem through the alternative optimization method. Specifically, we derive the optimal closed-form solution for time division policies through convex optimization techniques, develop a bisection method to address the optimal

bandwidth allocation policy, and use the set expansion algorithm to achieve the device scheduling policy.

- Experiments show that the proposed FL algorithm achieves faster convergence speed and higher model accuracies compared with the state-of-art FL algorithm in [21], improving 2.72% and 11.6% accuracy on MNIST and CIFAR-10 datasets<sup>1</sup>, respectively. Moreover, the proposed joint device scheduling and resource management algorithm can reduce around 29% energy budget or 20% time budget and is able to achieve higher accuracies than the considered benchmarks on the MNIST dataset. On the CIFAR-10 dataset, the proposed algorithm can obtain slight higher accuracies as the benchmark scheme but can reduce 25% energy budget or 12.5% time budget.

### C. Organization and Notations

The rest of this paper is organized as follows: In Section II, we introduce the FL system and learning cost, then formulate the global loss minimization problem. The convergence analysis and problem transformation are illustrated in Section III. The joint device schedule, wireless bandwidth allocation, and time division algorithm are developed in IV. Section V verifies the effectiveness of the proposed scheme by simulation. The conclusion is drawn in Section VI. For convenience, we use “ $\triangleq$ ” to denote “is defined to be equal to”,  $|\cdot|$  denote the size operation of a set,  $\nabla(\cdot)$  denote gradient operator,  $\langle \cdot, \cdot \rangle$  denote inner product operator, and “ $\|\cdot\|$ ” denote the  $\ell_2$  norm throughout this paper. The main notations used in this paper are summarized in Table I.

## II. SYSTEM MODEL

After introducing the general FL system in this section, we will discuss FL with partial model aggregation (PMA), the computation cost, and the communication cost, and then formulate the problem.

### A. Federated Learning System

In this work, we consider a typical FL setting for supervised learning, consisting of one PS and  $K$  devices indexed by  $\mathcal{K} = \{1, 2, \dots, K\}$ , as shown in Fig. 1. Each device  $k$  ( $k \in \mathcal{K}$ ) has a local dataset  $\mathcal{D}_k$  with  $D_k = |\mathcal{D}_k|$  data samples. Without loss of generality, we assume there

<sup>1</sup>MNIST: <http://yann.lecun.com/exdb/mnist/>, CIFAR-10: <https://www.cs.toronto.edu/~kriz/cifar.html>

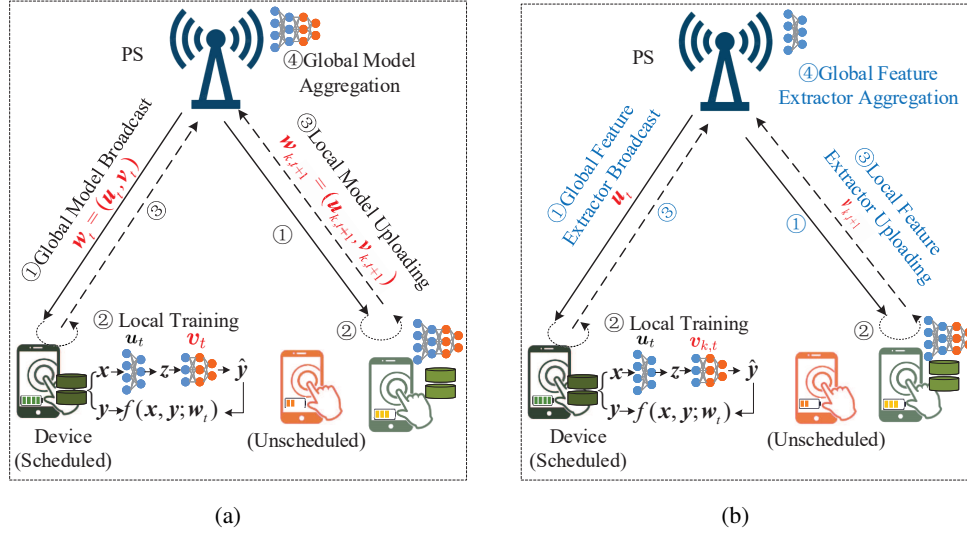


Fig. 1. Illustrating the federated learning system and mechanism: (a) shows the traditional federated learning mechanism which trains a global model (including feature extractor and predictor); and (b) presents the federated learning mechanism with collaboratively train a feature extractor while the predictor is trained by each device itself for personalization.

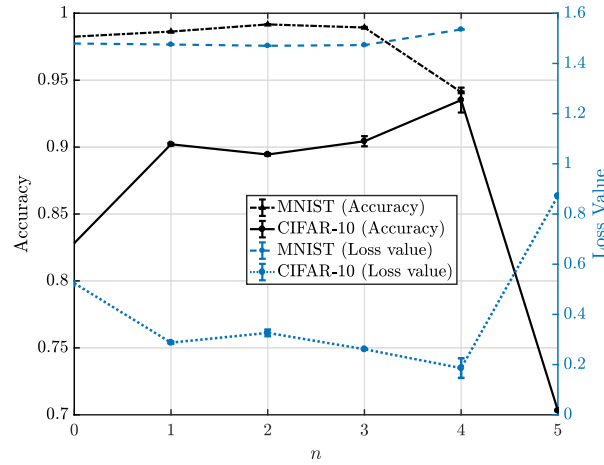


Fig. 2. The test accuracy and loss function value on MNIST and CIFAR-10 datasets, from without sharing parameters (each device solely train the model by using its own dataset) to sharing entire model parameters (FedAvg).

is no overlapping for datasets from different devices, i.e.,  $\mathcal{D}_k \cap \mathcal{D}_h = \emptyset, (\forall k, h \in \mathcal{K})$ . Thus, the whole dataset,  $\mathcal{D} = \cup \{\mathcal{D}_k\}_{k=1}^K$ , is with total number of samples  $D = \sum_{k=1}^K D_k$ .

Given a data sample  $(\mathbf{x}, \mathbf{y}) \in \mathcal{D}$ , where  $\mathbf{x} \in \mathbb{R}^d$  represents the input feature vector of the sample, and  $\mathbf{y} \in \mathbb{R}$  is the corresponding ground-truth label. Let  $\mathbf{z} \in \mathbb{R}^p$  be the latent feature space with  $p < d$ . The machine learning model parameterized by  $\mathbf{w} = [\mathbf{u}, \mathbf{v}]$  consists of two components: a feature extractor  $\mathbf{x} \rightarrow \mathbf{z}$  parameterized by  $\mathbf{u}$  and a predictor  $\mathbf{z} \rightarrow \hat{\mathbf{y}}$  parameterized by  $\mathbf{v}$ . Let  $f(\mathbf{x}, \mathbf{y}; \mathbf{w})$  denotes the sample-wise loss function, which quantifies the error between the ground-truth label,  $\mathbf{y}$ , and the predicted output,  $\hat{\mathbf{y}}$ , based on model  $\mathbf{w}$ . Thus, the local loss

TABLE I  
NOTATION SUMMARY

Notation	Definition	Notation	Definition
$\mathcal{K}; K;$	Set of devices; size of $\mathcal{K}$	$\mathcal{D}_k; D_k$	Local dataset of device $k$ ; size of $\mathcal{D}_k$
$F_k(\mathbf{u}_k, \mathbf{v}_k);$ $F(\mathbf{u}, \mathbf{V})$	Local loss function of device $k$ ; global loss function	$\mathbf{w}_k; \mathbf{u}_k; \mathbf{v}_k;$ $\mathbf{V}$	Local model; local feature extractor; local predictor of device $k$ ; all devices' predictors
$\mathcal{D}; D$	Overall dataset in the system; size of $\mathcal{D}$	$\eta_u; \eta_v$	Learning rate for feature extractor and predictor
$\mathbf{S}_t;$	Scheduling policy in round $t$ , i.e., the set of scheduled devices	$f_{k,t}; f_{k,\max}$	CPU frequency of device $k$ in round $t$ ; maximum CPU frequency of device $k$
$p_{k,t}; p_{k,\max}$	Transmit power of device $k$ in round $t$ ; maximum transmit power of device $k$	$C_k; Q$	Computation workload of one data sample at device $k$ ; Data size of feature extractor
$B; \theta_t$	Wireless transmission bandwidth; the proportion of $B$ allocated to devices in round $t$	$\mathbf{T}_t^L; \mathbf{T}_t^U$	Computation time and communication time for devices in round $t$
$E_k$	Total energy budget of device $k$ ;	$T_{\max}$	Maximum completion time for each round

function at device  $k$ , which measures the model error on its local dataset  $\mathcal{D}_k$ , is defined as

$$F_k(\mathbf{w}_k) = F_k(\mathbf{u}_k, \mathbf{v}_k) \triangleq \frac{1}{D_k} \sum_{(\mathbf{x}, \mathbf{y}) \in \mathcal{D}_k} f(\mathbf{x}, \mathbf{y}; \mathbf{w}_k), \quad (1)$$

where  $\mathbf{w}_k$  denotes the model of device  $k$ ;  $\mathbf{u}_k$  and  $\mathbf{v}_k$  correspond to the feature extractor and predictor, respectively. Accordingly, the global loss function associated with all distributed local datasets is given by

$$F(\mathbf{w}_1, \dots, \mathbf{w}_K) \triangleq \frac{1}{D} \sum_{k=1}^K D_k F_k(\mathbf{w}_k). \quad (2)$$

The federated learning process is done by solving the following problem

$$\min_{(\mathbf{w}_1, \dots, \mathbf{w}_K)} \left( F(\mathbf{w}_1, \dots, \mathbf{w}_K) \triangleq \frac{1}{D} \sum_{k=1}^K D_k F_k(\mathbf{w}_k) \right). \quad (3)$$

To preserve the data privacy of devices, the devices collaboratively learn  $(\mathbf{w}_1, \dots, \mathbf{w}_K)$  by only uploading local learning models  $\mathbf{w}_k (k \in \mathcal{K})$  to the PS for periodical aggregation, instead of transmitting the raw training data.

### B. Federated Learning with Partial Model Aggregation

The main objective of the typical federated learning algorithms, such as the FedAvg [20] and stochastic controlled averaging FL [24], is to find an optimal shared global model  $\mathbf{w}^* = \mathbf{w}_k^* (\forall k \in \mathcal{K})$  that minimizes the global loss function  $F(\mathbf{w}_1, \dots, \mathbf{w}_K)$ , as shown in Fig. 1(a). However, the data distributions among different devices in real-world FL systems are often heterogeneous, namely statistical heterogeneity. In the presence of statistical data heterogeneity, the local optimal models may drift significantly from each other, and thus solely optimizing for the global model's accuracy leads to a poor generalization of each device [6].

Fortunately, the success of centralized learning in training multiple tasks or learning multiple classes simultaneously has shown that data often shares a global feature representation (i.e.,  $\mathbf{u}$ ), while the statistical heterogeneity across devices or tasks is mainly located at the labels' predictor (i.e.,  $\mathbf{v}$ ) [22], [23]. Thus, this work proposes PMA in the FL training process instead of aggregating the entire model, as shown in 1(b). Specifically, devices who participate in the FL training process only upload the parameters of feature extractor  $\mathbf{u}$  for global aggregation and the predictor  $\mathbf{v}$  is localized for personalization. The learning process repeats the following steps until the model converges. The combination of the steps is referred to as a global round.

- **Device Selection:** The PS collects communication and computation information from each device and determines the set of scheduled devices in the current round, which is denoted by  $\mathcal{S}_t$ . Let  $\alpha_{k,t} \in \{0, 1\}$  denotes the scheduling indicator of device  $k$  in round  $t$ , where  $\alpha_{k,t} = 1$  indicates that device  $k$  is scheduled in round  $t$ ,  $\alpha_{k,t} = 0$  otherwise. Thus, we have  $\mathcal{S}_t = \{k : \alpha_{k,t} = 1, \forall k \in \mathcal{K}\}$ .
- **Global Feature Extractor Broadcast:** In each round  $t$ , the PS broadcasts the current latest global feature extractor  $\mathbf{u}_t$  to all scheduled devices.
- **Local Model Training:** All scheduled devices update their local models after receiving the global feature extractor  $\mathbf{u}_t$ . For device  $k$ , its local feature extractor in round  $(t + 1)$  is updated as
 
$$\mathbf{u}_{k,t+1} = \mathbf{u}_t - \alpha_{k,t} \eta_u \nabla_{\mathbf{u}} F_k(\mathbf{u}_t, \mathbf{v}_{k,t}), \quad (4)$$

and its predictor is updated by

$$\mathbf{v}_{k,t+1} = \mathbf{v}_{k,t} - \alpha_{k,t} \eta_v \nabla_{\mathbf{v}} F_k(\mathbf{u}_t, \mathbf{v}_{k,t}), \quad (5)$$

where  $\eta_u$  and  $\eta_v$  represent the learning rate of feature extractor  $\mathbf{u}$  and predictor  $\mathbf{v}$ , respectively. For ease of presentation, we use  $\mathbf{V} = (\mathbf{v}_1, \mathbf{v}_2, \dots, \mathbf{v}_K)$  denotes all the devices' predictors throughout this paper.

- **Global Feature Extractor Aggregation:** After finishing the local training, all scheduled devices upload their updated local feature extractors to the PS through wireless channels for aggregation. Specifically, the PS computes the global shared feature extractor as follows:

$$\mathbf{u}_{t+1} = \frac{\sum_{k=1}^K \alpha_{k,t} D_k \mathbf{u}_{k,t+1}}{\sum_{k=1}^K \alpha_{k,t} D_k}. \quad (6)$$

To better illustrate the benefits of partial sharing the model parameters, we provide an experiment on both MNIST and CIFAR-10 datasets in Fig. 2, where the data distribution of each device is non-IID. Specifically, each device possesses at most two classes of data samples and



participates in the training in each round. The MNIST dataset is trained by a 4-layers multi-layer perceptron (MLP) model, and the CIFAR-10 dataset is trained by a 5-layers convolutional neural network (CNN) model. The detailed configurations are shown in the experimental setting part in Section V. Fig. 2 shows that the MLP with only sharing the first two layers ( $n = 2$ ) in the training process obtains the highest accuracy and the CNN achieves the highest accuracy by aggregating the first four layers ( $n = 4$ ). One interesting result is that for both MLP and CNN, the global trained model ( $n = 4$  for the MLP and  $n = 5$  for the CNN) is less accurate than the local models of devices ( $n = 0$  for both the MLP and CNN) trained by their local datasets. Thus, aggregating the feature extractor with sufficient feature extracting ability in the training process is an efficient method to obtain better performance in the non-IID data distribution scenarios, instead of aggregating the entire model or solely training models on devices' local datasets.

### C. Computation Cost

In each global round  $t$ , the selected devices will perform local training after receiving the global feature extractor,  $\mathbf{u}_t$ , then uploading the trained local feature extractor parameters,  $\mathbf{u}_{k,t+1}$  ( $\forall k \in \mathcal{S}_t$ ), to the PS for aggregation. Let  $f_{k,t}$  denote the CPU frequency of device  $k$ . Employing dynamic voltage and frequency scaling techniques [11], device  $k$  can control the energy consumption for computation by adjusting the CPU frequency. Denote  $f_{k,\max}$  the maximum CPU frequency of device  $k$ . For any given machine learning model, the number of floating-point operations (FLOPs) required to one data sample for gradient calculation can be estimated, denoted by  $G$  [25]. Let  $\zeta_k$  denote the number of CPU cycles required to process one floating-point operation, which depends on the CPU. Thus, the computation workload of one data sample at device  $k$  is represented by  $C_k = \zeta_k G$ . Based on the real measurement result in [26], energy consumption by devices is proportional to the square of their frequency. Thus, given the computation time restriction,  $T_{k,t}^L$ , the most energy efficient CPU frequency is  $f_{k,t} = \frac{\tau D_k C_k}{T_{k,t}^L}$ , where  $\tau$  is the the number of local iterations. The corresponding energy consumption of device  $k$  to perform local training is

$$E_{k,t}^L = \kappa \tau D_k C_k f_{k,t}^2 = \frac{\kappa \tau^3 D_k^3 C_k^3}{(T_{k,t}^L)^2}, \quad (7)$$

where  $\kappa$  denotes the devices' energy coefficient that hinges on chip architecture. Since the CPU frequency of device  $k$  is restricted by  $f_{k,\max}$ , the computation time should satisfy

$$T_{k,t}^L \geq \frac{\tau D_k C_k}{f_{k,\max}}. \quad (8)$$

In the above discussion, we have ignored the global feature extractor aggregation cost, because the PS usually has strong computation capability with negligible aggregation delay.

#### D. Communication Cost

The frequency-division multiple access (FDMA) technique is employed in the FL system with a total available bandwidth of  $B$  Hz for devices to upload their local feature extractors  $\mathbf{u}_{k,t}$ . Let  $\theta_{k,t}$  ( $0 \leq \theta_{k,t} \leq 1$ ) represent the proportion of wireless channel bandwidth allocated to device  $k$  in round  $t$  and  $p_{k,t}$  denote the uplink transmission power of device  $k$  ( $k \in \mathcal{K}$ ). We assume that the channel gain,  $h_{k,t}$ , between device  $k$  and the PS remains unchanged within one round but varies independently and identically over rounds. Consequently, the achievable uplink rates for device  $k$  in round  $t$  can be characterized by Shannon capacity, i.e.,  $r_{k,t} = \theta_{k,t} B \log(1 + \frac{p_{k,t} h_{k,t}}{\theta_{k,t} B N_0})$ , where  $N_0$  is the power density of noise. Denote  $Q$  by the data size of feature extractor ( $\mathbf{u}_{k,t}, \forall k \in \mathcal{K}, \forall t$ ). Given the maximum communication time  $T_{k,t}^U$ , the most energy efficient transmission method is  $r_{k,t} = \frac{Q}{T_{k,t}^U}$  [27]. Thus, the transmit power is

$$p_{k,t} = \frac{\theta_{k,t} B N_0}{h_{k,t}} \left( 2^{\frac{Q}{\theta_{k,t} B T_{k,t}^U}} - 1 \right). \quad (9)$$

The corresponding energy consumption is  $E_{k,t}^U = p_{k,t} T_{k,t}^U$ . Thus, the total energy consumption of device  $k$  in round  $t$  for both computation and communication is  $E_{k,t} = E_{k,t}^L + E_{k,t}^U$ . Let  $p_{k,\max}$  denote the maximum transmit power of device  $k$ , then  $0 \leq p_{k,t} \leq p_{k,\max}$ . Thus, the communication time for device  $k$  uploading its local feature extractor should satisfy

$$T_{k,t}^U \geq \frac{Q}{\theta_{k,t} B \log \left( 1 + \frac{p_{k,\max} h_{k,t}}{\theta_{k,t} B N_0} \right)}. \quad (10)$$

Similar to many existing works as in [8], [11]–[13], we ignore the global feature extractor broadcasting cost and mainly focus on the performance bottleneck of the battery and communication-constrained edge devices because the PS usually supplied by the grid is energy-sufficient. Moreover, the broadcasting process occupies the entire bandwidth and the transmit power of the PS is usually large, the transmission delay is negligible.

#### E. Problem Formulation

The objective of this work is to minimize the expected global loss  $\mathbb{E}[F(\mathbf{u}_T, \mathbf{V}_T)]$  after  $T$  rounds under the energy budget constraints of devices. To this end, we jointly optimize the device scheduling, bandwidth allocation, computation time, and communication time allocation policy.

Denote  $\boldsymbol{\theta}_t = (\theta_{1,t}, \theta_{2,t}, \dots, \theta_{K,t})$  as the proportions of the overall wireless bandwidth allocated to different devices in round  $t$ . Let  $\mathbf{T}_t^L = (T_{1,t}^L, T_{2,t}^L, \dots, T_{K,t}^L)$  and  $\mathbf{T}_t^U = (T_{1,t}^U, T_{2,t}^U, \dots, T_{K,t}^U)$  denote the computation time and communication time for all devices in round  $t$ , respectively.

We formulate the problem as follows:

$$\mathcal{P} : \min_{\{\mathbf{s}_t, \boldsymbol{\theta}_t, \mathbf{T}_t^L, \mathbf{T}_t^U\}_{t=0}^{T-1}} \mathbb{E}[F(\mathbf{u}_T, \mathbf{V}_T)] \quad (11)$$

$$\text{s. t. } (8), (10), \quad (11a)$$

$$\sum_{t=0}^{T-1} E_{k,t} \leq E_k, \forall k \in \mathcal{K}, \quad (11b)$$

$$\alpha_{k,t} \in \{0, 1\}, \forall k \in \mathcal{K}, \forall t. \quad (11c)$$

$$\sum_{k=1}^K \theta_{k,t} \leq 1, \forall t, \quad (11d)$$

$$0 \leq \theta_{k,t} \leq 1, \forall k \in \mathcal{K}, \forall t, \quad (11e)$$

$$T_{k,t}^L + T_{k,t}^U \leq T_{\max}, \forall k \in \mathcal{K}, \forall t, \quad (11f)$$

In problem  $\mathcal{P}$ , (11a) restricts the computation and communication time. (11b) indicates that for each device, the total energy consumption for both computation and communication over  $T$  global rounds cannot exceed its given budget. (11c) indicates that which devices are scheduled in each round. (11d) assures that the wireless bandwidth resource allocated to all devices would not exceed the total available bandwidth resource. (11e) imposes restrictions on the wireless bandwidth resource allocated to each device. (11f) stipulates that the completion time for the participating devices in one round cannot exceed its maximum allowable delay  $T_{\max}$ .

Problem  $\mathcal{P}$  involves a combinatorial optimization over the multi-dimensional discrete and continuous space, which is challenging to solve. Two major challenges of solving problem  $\mathcal{P}$  are:

1) **Inexplicit form of the objective function:** Since the evolutions of the feature extractor  $\mathbf{u}_t$  and predictors  $\mathbf{v}_{k,t}$  are complex in the training process, it is intractable to solve the close-form expression of  $\mathbb{E}[F(\mathbf{u}_T, \mathbf{V}_T)]$ .

2) **Unknown future information:** The optimal solution of  $\mathcal{P}$  requires exact channel state and devices' energy status information of all rounds at the beginning of training, which is impractical in real-world systems.

To tackle these challenges, we first analyze the convergence bound of the considered PMA-FL algorithm and transform problem  $\mathcal{P}$  into optimizing the convergence bound.

### III. CONVERGENCE ANALYSIS AND PROBLEM TRANSFORMATION

In this section, we start with convergence analysis of the considered PMA-FL algorithm to find a metric, termed scheduled data sample volume (SDSV), which is in an explicit form with respect to the device schedule. Then, we transform problem  $\mathcal{P}$  into maximizing this metric, so as to obtain the minimum global loss function when the FL converges. To address the challenge brought by the long-term energy constraint, we further transform the problem into a deterministic problem in each communication round by characterizing the Lyapunov drift-plus-penalty ratio function with the assistance of the Lyapunov optimization framework.

#### A. Convergence Analysis

We now investigate the convergence behaviour of the federated learning algorithm with partial aggregation. To facilitate analysis, we make the following assumptions on the loss functions  $F(\cdot)$ .

*Assumption 1.* (Lipschitz continuous): All loss function  $F_k(\mathbf{u}, \mathbf{v}_k)$  are continuously differentiable with respect to  $\mathbf{u}$  and  $\mathbf{v}_k$ , and there exist constants  $L_u$ ,  $L_v$ ,  $L_{uv}$ , and  $L_{vu}$  such that for each  $F_k(\mathbf{u}, \mathbf{v}_k)$  ( $k \in \mathcal{K}$ ),

- $\nabla_{\mathbf{u}} F_k(\mathbf{u}, \mathbf{v}_k)$  is  $L_u$ -Lipschitz continuous with  $\mathbf{u}$  and  $L_{uv}$ -Lipschitz continuous with  $\mathbf{v}_k$ , that is,

$$\|\nabla_{\mathbf{u}} F_k(\mathbf{u}, \mathbf{v}_k) - \nabla_{\mathbf{u}} F_k(\mathbf{u}', \mathbf{v}_k)\| \leq L_u \|\mathbf{u} - \mathbf{u}'\|, \quad (12)$$

and

$$\|\nabla_{\mathbf{u}} F_k(\mathbf{u}, \mathbf{v}_k) - \nabla_{\mathbf{u}} F_k(\mathbf{u}, \mathbf{v}_k')\| \leq L_{uv} \|\mathbf{v}_k - \mathbf{v}_k'\|. \quad (13)$$

- $\nabla_{\mathbf{v}} F_k(\mathbf{u}, \mathbf{v}_k)$  is  $L_v$ -Lipschitz continuous with  $\mathbf{v}_k$  and  $L_{vu}$ -Lipschitz continuous with  $\mathbf{u}$ .

*Assumption 2.* (Partial Gradient Diversity): There exist  $\delta \geq 0$  and  $\rho \geq 0$  such that for all  $\mathbf{u}$  and  $\mathbf{V}$ , i.e.,

$$\|\nabla_{\mathbf{u}} F_i(\mathbf{u}, \mathbf{v}_k)\|^2 \leq \delta^2 + \rho^2 \|\nabla_{\mathbf{u}} F(\mathbf{u}, \mathbf{V})\|^2. \quad (14)$$

Assumption 1 is not stringent, which is satisfied by most deep neural networks. In fact, the convolution layer, linear layer, and some nonlinear activation functions (e.g., Sigmoid, tanh and Rectified Linear Unit (ReLU)) have already proved to be Lipschitz [28]. Based on [29], a deep neural network defined by a composition of functions is a Lipschitz neural network if the functions in all layers are Lipschitz. Thus, most neural networks have the Lipschitz continuous gradients. However, the exact computation of the Lipschitz constant of deep learning architectures

is intractable, even for two-layer neural networks [30]. Assumption 2 is widely used in the convergence analysis in FL algorithms, e.g., [14], [24], [31]. To begin with, we first derive a key lemma, proved in Appendix A, to assist our analysis as follows:

**Lemma 1.** *Let Assumption 1 holds, we have*

$$F(\mathbf{u}_{t+1}, \mathbf{V}_{t+1}) - F(\mathbf{u}_t, \mathbf{V}_t) \leq \langle \nabla_{\mathbf{u}} F(\mathbf{u}_t, \mathbf{V}_t), \mathbf{u}_{t+1} - \mathbf{u}_t \rangle + \frac{1+\chi}{2} L_{\mathbf{u}} \|\mathbf{u}_{t+1} - \mathbf{u}_t\|^2 \\ + \frac{1}{D} \sum_{k=1}^K D_k \left( \langle \nabla_{\mathbf{v}} F_k(\mathbf{u}_t, \mathbf{v}_{k,t}), \mathbf{v}_{k,t+1} - \mathbf{v}_{k,t} \rangle + \frac{1+\chi}{2} L_{\mathbf{v}} \|\mathbf{v}_{k,t+1} - \mathbf{v}_{k,t}\|^2 \right), \quad (15)$$

where  $\chi = \max\{L_{\mathbf{u}\mathbf{v}}, L_{\mathbf{v}\mathbf{u}}\} / \sqrt{L_{\mathbf{u}} L_{\mathbf{v}}}$ , which measures the relative cross-sensitivity of  $\nabla_{\mathbf{u}} F_k(\mathbf{u}, \mathbf{v}_k)$  with respect to  $\mathbf{v}_k$  and  $\nabla_{\mathbf{v}} F_k(\mathbf{u}, \mathbf{v}_k)$  with respect to  $\mathbf{u}$ .

Based on Lemma 1, we derive the one-round global loss reduction bound in Appendix B, which is summarized in the following Lemma.

**Lemma 2.** *Let Assumption 1 and Assumption 2 hold. The learning rate satisfy  $\eta_{\mathbf{u}} \leq \frac{1}{(\chi+1)L_{\mathbf{u}}}$ ,  $\eta_{\mathbf{v}} \leq \frac{2}{(\chi+1)L_{\mathbf{v}}}$ , we have*

$$\mathbb{E}[F(\mathbf{u}_{t+1}, \mathbf{V}_{t+1}) - F(\mathbf{u}_t, \mathbf{V}_t)] \leq \frac{1}{2} \eta_{\mathbf{u}} \left( \frac{4}{D^2} \left( D - \sum_{k=1}^K \alpha_{k,t} D_k \right)^2 \rho^2 - 1 \right) \mathbb{E} \|\nabla_{\mathbf{u}} F(\mathbf{u}_t, \mathbf{V}_t)\|^2 \\ + 2\eta_{\mathbf{u}} \frac{\left( D - \sum_{k=1}^K \alpha_{k,t} D_k \right)^2 \delta^2}{D^2}. \quad (16)$$

According to Lemma 2, one can find that the number of data samples scheduled in each round, i.e.,  $\sum_{k=1}^K \alpha_{k,t} D_k$ , is the main contributor to the convergence rate of training. Based on Lemma 2, we derive the convergence performance of the proposed PMA-FL algorithm after  $T$  training rounds in the following theorem, proved in Appendix C.

**Theorem 1.** *Let Assumption 1 and Assumption 2 hold. The learning rate satisfy  $\eta_{\mathbf{u}} \leq \frac{1}{(\chi+1)L_{\mathbf{u}}}$ ,  $\eta_{\mathbf{v}} \leq \frac{2}{(\chi+1)L_{\mathbf{v}}}$ , the convergence bound in the  $T$ -th global round is given by*

$$\mathbb{E}[F(\mathbf{u}_T, \mathbf{V}_T) - F(\mathbf{u}^*, \mathbf{V}^*)] \leq \left( \mathbb{E}[F(\mathbf{u}_0, \mathbf{V}_0) - F(\mathbf{u}^*, \mathbf{V}^*)] \right) \prod_{t=0}^{T-1} A_t \\ + \sum_{t=0}^{T-1} \frac{2\eta_{\mathbf{u}} \delta^2}{D^2} \left( D - \sum_{k=1}^K \alpha_{k,t} D_k \right)^2 \prod_{j=t+1}^{T-1} A_j, \quad (17)$$

where  $A_t = 1 + \eta_{\mathbf{u}} L_{\mathbf{u}} \left( \frac{4}{D^2} \left( D - \sum_{k=1}^K \alpha_{k,t} D_k \right)^2 \rho^2 - 1 \right)$ .

Theorem 1 indicates that the expected gap between the global loss value after  $T$  rounds and

the optimal one is bounded by two terms: 1) the expected gap in the initial round, 2) the cumulate impact of data sample scheduling on model convergence. As  $T$  increases, the former converges to zero because  $\prod_{t=0}^{T-1} A_t$  turns to 0 and the latter approaches to be fixed. In addition, increasing  $\sum_{k=1}^K \alpha_{k,t} D_k$  in each round is able to reduce the global loss function. A larger  $\sum_{k=1}^K \alpha_{k,t} D_k$  helps  $\prod_{t=0}^{T-1} A_t$  approach to 0 faster and thus improving the learning efficiency.

### B. Problem Transformation

Motivated by Theorem 1, we define  $\sum_{t=0}^{T-1} \sum_{k=1}^K \alpha_{k,t} D_k$  as SDSV and maximize it for the global loss function minimization. Thus, we transform problem  $\mathcal{P}$  into the following one.

$$\begin{aligned} \mathcal{P}_1 : \quad & \max_{\{\mathbf{S}_t, \mathbf{T}_t^L, \mathbf{T}_t^U, \boldsymbol{\theta}_t\}_{t=0}^{T-1}} \sum_{t=0}^{T-1} \sum_{k=1}^K \alpha_{k,t} D_k \\ \text{s. t.} \quad & (8), (10), (11b), (11c), (11d), (11e), (11f). \end{aligned} \quad (18)$$

Problem  $\mathcal{P}_1$  is difficult to solve due to the long-term energy constraint and the unknown future information about channel condition for devices. To enable online dynamic scheduling for devices, we construct a virtual queue  $q_k(t)$  for each device  $k$  to indicate the gap between the cumulative energy consumption till round  $t$  and the budget, evolving according to

$$q_k(t+1) = \max \left\{ q_k(t) + \alpha_{k,t} E_{k,t} - \frac{E_k}{T}, 0 \right\}, \quad (19)$$

with an initial value  $q_k(0) = 0$  for all devices. Inspired by the drift-plus-penalty algorithm of Lyapunov optimization [32], the online scheduling aims to solve the following problem,

$$\begin{aligned} \mathcal{P}_2 : \quad & \min_{\{\mathbf{S}_t, \mathbf{T}_t^L, \mathbf{T}_t^U, \boldsymbol{\theta}_t\}} -V \sum_{k=1}^K \alpha_{k,t} D_k + \sum_{k=1}^K q_k(t) \alpha_{k,t} E_{k,t} \\ \text{s. t.} \quad & (8), (10), (11c), (11d), (11e), (11f). \end{aligned} \quad (20)$$

where  $V \geq 0$  is an adjustable weight parameter to balance SDSV and energy consumption. A large  $V$  indicates that the optimization objective emphasizes more on the scheduled data samples and less on energy consumption minimization, and vice visa.

## IV. ENERGY-EFFICIENT DYNAMIC DEVICE SCHEDULING AND RESOURCE MANAGEMENT

In this section, we solve the deterministic combinatorial problems  $\mathcal{P}_2$  in each communication round. We first exploit the dependences among  $\mathbf{S}_t$ ,  $\boldsymbol{\theta}_t$ ,  $\mathbf{T}_t^L$ , and  $\mathbf{T}_t^U$  in problem  $\mathcal{P}_2$  and transform it into an equivalent problem that joint optimizing  $\mathbf{S}_t$ ,  $\boldsymbol{\theta}_t$ , and  $\mathbf{T}_t^L$ . Then we decompose it into three

sub-problems and deploy an alternative optimization technique to obtain its optimal solution. For the convenience of analysis, we rewrite the local feature extractor uploading energy consumption as

$$E_{k,t}^U = p_{k,t} T_{k,t}^U = \frac{\theta_{k,t} B N_0 T_{k,t}^U}{h_{k,t}} \left( 2^{\frac{Q}{\theta_{k,t} B T_{k,t}^U}} - 1 \right), \quad (21)$$

which is a non-increasing function with respect to  $T_{k,t}^U$ . Thus, by taking into account the constraint (11f), the optimal communication time satisfies  $T_{k,t}^U = T_{\max} - T_{k,t}^L$ . Based on this, we can simplify problem  $\mathcal{P}_2$  as the following equivalent problem,

$$\mathcal{P}_3 : \min_{\{s_t, \theta_t, T_t^L\}} -V \sum_{k=1}^K \alpha_{k,t} D_k + \sum_{k=1}^K q_k(t) \alpha_{k,t} E_{k,t} \quad (22)$$

$$\text{s. t.} \quad (11c), (11d), (11e),$$

$$\frac{\tau D_k C_k}{f_{k,\max}} \leq T_{k,t}^L \leq T_{\max} - \frac{Q}{r_{k,t}^{\max}(\theta_{k,t})}, \quad (22a)$$

where

$$r_{k,t}^{\max}(\theta_{k,t}) = \theta_{k,t} B \log \left( 1 + \frac{p_{k,\max} h_{k,t}}{\theta_{k,t} B N_0} \right). \quad (23)$$

However, problem  $\mathcal{P}_3$  is a mixed integer non-linear programming problem, which is still difficult to solve. In the below, we decompose it into three sub-problems and solve them one by one.

#### A. Optimal Local Training Time Allocation

For any given device scheduling policy  $S_t$  and bandwidth allocation strategy  $\theta_t$ , we can decompose the computation time allocation problem as follows,

$$\mathcal{P}_4 : \min_{T_t^L} \sum_{k \in S_t} q_k(t) E_{k,t} \quad (24)$$

$$\text{s. t.} \quad (22a).$$

We can prove that  $\mathcal{P}_4$  is convex, and obtain its optimal solution as summarized in Lemma 3, proved in Appendix D.

**Lemma 3.** *Problem  $\mathcal{P}_4$  is a convex problem and its optimal solution is given as*

$$T_{k,t}^{L,*} = \begin{cases} \frac{\tau D_k C_k}{f_{k,\max}}, & T_{k,t}^{L,0} \leq \frac{\tau D_k C_k}{f_{k,\max}}, \\ T_{\max} - \frac{Q}{r_{k,t}^{\max}(\theta_{k,t})}, & T_{k,t}^{L,0} \geq T_{\max} - \frac{Q}{r_{k,t}^{\max}(\theta_{k,t})}, \\ T_{k,t}^{L,0}, & \text{otherwise.} \end{cases} \quad (25)$$

where  $T_{k,t}^{L,0}$  satisfies the equality  $\frac{\partial E_{k,t}}{\partial T_{k,t}^{L,0}} = 0$ .

In fact, constraint (22a) imposes restrictions on the maximum frequency and transmit power and is usually inactive in practical system design because this usually can be satisfied by modifying the minimum required latency constraint,  $T_{\max}$ , and bandwidth  $B$ . Thus, we have the following remark.

*Remark 1.* In general, the optimal computation time satisfy  $T_{k,t}^{L,*} = T_{k,t}^{L,0}$ , which is equivalent to  $\frac{\partial E_{k,t}^L}{\partial T_{k,t}^L} = \frac{\partial E_{k,t}^U}{\partial T_k^U}$ . In other words, the computation time allocation policy is optimal when the power of local training equals that of wireless communication.

### B. Optimal Wireless Bandwidth Allocation

For ease of presentation, we define an auxiliary function for each device  $k \in \mathcal{K}$  as follows:

$$g_k(\theta_{k,t}) = \exp\left(\frac{Q \ln 2}{\theta_{k,t} B(T_{\max} - T_{k,t}^L)}\right) - 1. \quad (26)$$

For any given computation time allocation decision  $\mathbf{T}_t^L$  and device scheduling policy  $\mathbf{S}_t$ , the wireless bandwidth allocation problem can be separated as,

$$\mathcal{P}_5 : \min_{\boldsymbol{\theta}_t} h(\boldsymbol{\theta}_t) \quad (27)$$

$$\text{s. t.} \quad (11d), (11e),$$

$$\frac{Q}{T_{\max} - T_{k,t}^L} \leq r_{k,t}^{\max}(\theta_{k,t}), \quad (27a)$$

where

$$h(\boldsymbol{\theta}_t) = \sum_{k \in \mathbf{S}_t} \theta_{k,t} \frac{N_0 B q_k(t) (T_{\max} - T_{k,t}^L)}{h_{k,t}} g_k(\theta_{k,t}). \quad (28)$$

Problem  $\mathcal{P}_5$  is a standard convex optimization problem, its proof is similar to that for Lemma 3 and thus omitted for brevity. Applying Karush-Kuhn-Tucker condition [33], the optimal solution for  $\boldsymbol{\theta}_t$  satisfies

$$\frac{\partial h(\boldsymbol{\theta}_t)}{\partial \theta_{k,t}} = -\lambda^*, \forall k \in \mathbf{S}_t, \quad (29)$$

where  $\lambda^*$  is the optimal Lagrange multiply and  $\sum_{k \in \mathbf{S}_t} \theta_{k,t} = 1$ . Thus, for each device  $k$ , we have

$$g_k(\theta_{k,t}) + \theta_{k,t} g'_k(\theta_{k,t}) = \frac{-\lambda^* h_{k,t}}{q_k(t) N_0 B (T_{\max} - T_{k,t}^L)}, \quad (30)$$

its inverse function is

$$\theta_{k,t}(\lambda^*) = \frac{Q \ln 2}{B(T_{\max} - T_{k,t}^L) \left( \mathcal{W}\left(\frac{\lambda^* h_{k,t}}{q_k(t) N_0 B (T_{\max} - T_{k,t}^L) e} - \frac{1}{e}\right) + 1 \right)}, \quad (31)$$



where  $\mathcal{W}$  refers to the principal branch of the Lambert  $\mathcal{W}$  function, defined as the solution for  $\mathcal{W}(x)e^{\mathcal{W}(x)} = x$ , in which  $e$  refers to the Euler's number.

In (31), there still exists an unknown variable  $\lambda^*$ . The value of  $\lambda^*$  is determined by the equation  $\sum_{k=1}^K \theta_{k,t}(\lambda^*) = 1$ . Since the expression of  $\theta_{k,t}(\lambda^*)$  is complicated, it is difficult to solve the optimal  $\lambda^*$ . Below we propose a bisection search method to solve  $\sum_{k=1}^K \theta_{k,t}(\lambda^*) = 1$ . To proceed, we have the following Proposition.

**Proposition 1.**  $\theta_{k,t}(\lambda)$  is a monotonically decreasing function with respect to  $\lambda$ .

*Proof.* Since the Lagrange multiply  $\lambda > 0$ , we have  $\frac{\lambda h_{k,t}}{eq_k(t)N_0B(T_{\max}-T_{k,t}^L)} - \frac{1}{e} > -\frac{1}{e}$ . Moreover,  $\mathcal{W}(x)$  is a monotonically increasing function when  $x \geq -\frac{1}{e}$ . Thus,  $\theta_{k,t}(\lambda)$  is a monotonically decreasing function with respect to  $\lambda$ .  $\square$

Based on Proposition 1, the bisection search method is employed to solve the equation. In the following, we derive the bisection search upper and lower bound on  $\lambda$ . Since  $\lambda > 0$ , the lower bound of  $\lambda$  is  $\lambda_{\text{LB}} = 0$ . For deriving the upper bound, we have  $\max_{k \in \mathcal{S}_t} \{\theta_{k,t}(\lambda)\} \geq 1/|\mathcal{S}_t|$ , thus

$$\mathcal{W}\left(\frac{\lambda h_{k,t}}{q_k(t)N_0B(T_{\max}-T_{k,t}^L)e} - \frac{1}{e}\right) \leq \frac{|\mathcal{S}_t|Q \ln 2}{B(T_{\max}-T_{k,t}^L)} - 1. \quad (32)$$

Let  $\varphi_k = \frac{|\mathcal{S}_t|Q \ln 2}{B(T_{\max}-T_{k,t}^L)}$ , from the definition of Lambert  $\mathcal{W}$  function, we have

$$\lambda_{\text{UB}} = \max_{k \in \mathcal{S}_t} \left\{ \frac{q_k(t)N_0B(T_{\max}-T_{k,t}^L) ((\varphi_k-1)e^{\varphi_k}+1)}{h_{k,t}} \right\}. \quad (33)$$

According to the lower bound  $\lambda_{\text{LB}}$  and upper bound  $\lambda_{\text{UB}}$ , the optimal Lagrange multiply,  $\lambda^*$ , can be solved by using the bisection search method. Furthermore, the optimal wireless bandwidth allocation policy  $\theta_t$  can be derived from (31). Based on the above analysis, we have the following remark.

*Remark 2.* From (29), when the bandwidth allocation policy is optimal, all devices' energy consumption-bandwidth rates (i.e.,  $\frac{\partial h(\theta_t)}{\partial \theta_{k,t}}$ ) are equal. This actually achieves the energy consumption balance between devices. Moreover, similar to the proof of Proposition 1, it can be proved that the optimal bandwidth form in (31) is monotonically decreasing with  $h_{k,t}$  and increasing with  $q_k(t)$ . Thus, more bandwidth should be allocated to the devices with weaker channels (smaller  $h_{k,t}$ ) and less remaining energy budgets (larger  $q_k(t)$ ).

### C. Device Scheduling Policy

Until now, for any given  $\mathbf{S}_t$ , the optimal solution for computation time allocation or wireless bandwidth allocation can be addressed if one of them is fixed. Below we solve the joint optimal solution for computation time and wireless bandwidth allocation. For clarity, we formulate the joint computation time allocation and bandwidth allocation problem under given device scheduling decision  $\mathbf{S}_t$  as follows:

$$\begin{aligned} \mathcal{P}_6 : \min_{\{\boldsymbol{\theta}_t, \mathbf{T}_t^L\}} & \sum_{k \in \mathbf{S}_t} q_k(t) E_{k,t} \\ \text{s. t.} & \quad (11d), (11e), (22a), \end{aligned} \quad (34)$$

which is a combination problem of  $\mathcal{P}_4$  and  $\mathcal{P}_5$ . Building on the preceding results, the computation time allocation problem,  $\mathcal{P}_4$ , and the bandwidth allocation problem,  $\mathcal{P}_5$ , are both convex optimization problems, problem  $\mathcal{P}_6$  is also a convex optimization problem. Thus, we solve the joint computation time and wireless bandwidth allocation policies via iterations [34] between problem  $\mathcal{P}_4$  and problem  $\mathcal{P}_5$ . Each iteration consists of two steps: (1) solving the optimal solution of problem  $\mathcal{P}_5$  for given  $\mathbf{T}_t^L$ ; (2) solving the optimal computation time allocation policy  $\mathbf{T}_t^L$  based on the obtained bandwidth allocation solution  $\boldsymbol{\theta}_t$ . The two steps are iterated until convergence. For clarity, we summarize the detailed steps on joint optimization of computation time and wireless bandwidth in Algorithm 1. Based on the complexity analysis results in [34], the time complexity of Algorithm 1 is  $\mathcal{O}(2K^{3.5})$

---

**Algorithm 1** Optimal Computation time and Bandwidth Allocation

---

- 1: Initialize  $\mathbf{S}_t$ , the computation time as  $\tilde{T}_t^L$ , and bandwidth allocation policy  $\boldsymbol{\theta}_t$ , the tolerant error  $\Upsilon > 0$
  - 2: Calculate the objective function value (20), denote as  $\mathcal{B}_0$
  - 3: **repeat**
  - 4:   Calculate the upper bound of the Lagrange multiply  $\lambda_{UB}$  based on (33), and let  $\lambda_{LB} = 0$
  - 5:   Utilize the bisection search method to solve the optimal bandwidth allocation policy  $\boldsymbol{\theta}_t$
  - 6:   Solve the optimal computation time allocation policy based on the obtained  $\boldsymbol{\theta}_t$  by using (25), update  $\tilde{T}_t^L$
  - 7:   Calculate the objective function value (34) of  $\mathbf{S}_t$  by substituting the obtained  $\tilde{T}_t^L$  and  $\boldsymbol{\theta}_t$ , denote as  $\mathcal{B}_1$
  - 8:    $\Delta = \mathcal{B}_0 - \mathcal{B}_1$ , update  $\mathcal{B}_0 = \mathcal{B}_1$
  - 9: **until**  $\Delta \leq \Upsilon$
  - 10: **return** The computation time allocation policy  $\tilde{T}_t^L$  and bandwidth allocation policy  $\boldsymbol{\theta}_t$
- 

Through the above analysis, we can solve the optimal value of the objective function in (22) for any given device scheduling decision  $\mathbf{S}_t$ . An intuitive method to solve the optimal device

scheduling solution is to solve the objective function value of all the possible device scheduling decisions first and then select the one with the minimum objective function value. However, this method has exponential time complexity  $\mathcal{O}(K^{3.5} \times 2^{K+1})$  since there are total  $\sum_{n=0}^K C_K^n = 2^K$  possible device scheduling decisions. To tackle this challenge, we have the following designs.

According to the objective function (22), it is desirable to select devices with small  $q_k(t)$  and  $E_{k,t}$ . The small  $E_{k,t}$  can be achieved by strong channels or/and high computation efficiencies. To identify such devices, we first perform equal bandwidth allocation over all devices and then evaluate the resulting energy consumption of each device  $\bar{E}_{k,t}$ . Specifically, each device  $k$  is allocated the same portion,  $\theta_{k,t} = \frac{1}{K}$ , of the total bandwidth  $B$ , and then solve problem  $\mathcal{P}_4$  to obtain the computation time allocation policy  $\mathbf{T}_t^L$ . Then, by substituting  $\theta_{k,t} = \frac{1}{K}$  and  $\mathbf{T}_t^L$  into the (7) and (21), the estimated energy consumption is calculated as  $\bar{E}_{k,t} = E_{k,t}^U + E_{k,t}^L$ .

Based on the evaluated energy consumption  $\bar{E}_{k,t}$ , we sort  $\mathcal{C}_{k,t} = q_k(t)\bar{E}_{k,t}$  in the ascending order, and then use the set expansion algorithm [11] to solve the optimal device selection policy by incrementally adds devices into the selection set,  $S$ . Firstly, the devices with  $q_k(t) = 0$  are all added into  $S$ , denote this device set by  $S_0$ . Next, the devices with  $q_k(t) > 0$  are added into  $S$  one by one in the ascending order of  $\mathcal{C}_{k,t}$ . For each possible device scheduling set  $S$ , we perform Algorithm 1 to obtain the optimal computation time and wireless bandwidth allocation decisions. Let  $\mathcal{R}^*(S) = (\theta^*(S), T^*(S))$  denote the optimal time and wireless bandwidth decision and  $\mathcal{Y}(S)$  represent the corresponding optimal objective function value of  $S$ , respectively. Denote  $\mathcal{H}$  as the set of all possible device scheduling set  $S$ .

Note that,  $\mathcal{Y}(S_0) = -V \sum_{k \in S_0} D_k$  due to  $q_k(t) = 0$  ( $\forall k \in S_0$ ). Since the energy consumption of users in  $S_0$  does not affect the objective function value, the minimum band required bandwidth should be allocated to them for saving more bandwidth resources for other users in  $(S - S_0)$ . Moreover, we add the users with  $q_k(t) > 0$  one by one into  $S$  and solve the optimal  $\mathcal{R}^*(S)$  and  $\mathcal{Y}(S)$ . For  $S$ , if its optimal computation time and wireless bandwidth allocation policy results in  $-VD_k + q_k(t)E_{k,t} > 0$  for the last added device  $k$ , we stop adding devices into  $S$  and remove the last added device. Then, we obtain the optimal device scheduling policy through comparing the objective function value of all  $S \in \mathcal{H}$ , i.e.,  $S_t^* = \arg \min_{S \in \mathcal{H}} \mathcal{Y}(S)$ . The optimal computation time and optimal bandwidth allocation policy correspond to  $T_t^*(S)$  and  $\theta_t^*(S)$ . For clarity, we summarize the detail steps of optimal device selection in Algorithm 2, which obtains the optimal solution of problem  $\mathcal{P}_1$  by solving at most  $K$  times convex problem  $\mathcal{P}_6$  and has polynomial time complexity  $\mathcal{O}(2K^{4.5})$ , which is smaller than  $\mathcal{O}(K^{3.5} \times 2^{K+1})$  when  $K > 1$ .

---

**Algorithm 2** Optimal Device scheduling

---

```

1: Input the virtual queue length  $q_k(t)$  ( $k \in \mathcal{K}$ ), initialize  $V$ 
2: Sort  $\mathcal{C}_{k,t}$  in ascending order.
3: Set  $S_0 = \{k : q_k(t) = 0\}$ ,  $S = S_0$  and  $\mathcal{H} = \{S_0\}$ 
4: for  $k = |S_0|+1, \dots, K$  do
5:   Update  $S = S \cup \{k\}$ 
6:   Solve the optimal computation time and bandwidth allocation policy by Algorithm 1, i.e.,  $\mathcal{R}(S) = (T_t^L, \theta_t)$ .

7:   if  $-VD_k + q_k(t)E_{k,t} > 0$  then
8:     Break the circulation
9:   else
10:    Add  $S$  into  $\mathcal{H}$ , i.e.,  $\mathcal{H} = \mathcal{H} \cup S$ 
11:   end if
12: end for
13: Find the optimal device scheduling set  $S_t^* = \arg \min_{S \in \mathcal{H}} \mathcal{V}(S)$ 
14: return The optimal device scheduling set  $S_t^*$ , computation time  $T_t^L$  and wireless bandwidth allocation  $\theta_t$ 

```

---

## V. NUMERICAL RESULTS

In this section, we evaluate the performance of the proposed energy-efficient dynamic device scheduling FL algorithm. In the simulation, all the codes are implemented in python 3.8 and Pytorch, running on a Linux server. We first present the evaluation setup and then show experimental results.

### A. Experimental Setting

The default experiment settings are given as follows unless specified otherwise.

1) **Datasets and Models:** We evaluate the proposed algorithm for an image classification task using MNIST and CIFAR-10 datasets. The MNIST dataset consists of 60,000 and 10,000 grey-valued digital images for training and test, respectively. Each image is a handwritten digital between 0 and 9 displayed as a  $28 \times 28$  pixel matrix. The CIFAR-10 dataset consists of 60000  $32 \times 32$  colour images in 10 classes, with 50000 training images and 10000 test images. For both MNIST and CIFAR-10, we first classify the training data samples according to their labels, then randomly split each class of data samples into  $2K/10$  shards, finally randomly distribute two shards of data samples to each device. For the MNIST dataset, we train a MLP, which consists of 4 layers with 550346 parameters in total. The first four layers have 784, 512, 256, and 64 units, respectively. Each of these layers is activated by the ReLU function. The last

layer is a 10-unit softmax output layer. For the MLP, the number of FLOPs required to one data sample for gradient calculation is equal to its parameters' number. In our proposed FL approach, devices only share parameters of the first 2 layers, which has 533504 parameters, accounting for 96.7% of the entire model parameters. For the CIFAR-10 dataset, we train a CNN with the following structure: two  $5 \times 5$  convolution layers each with 64 channels and followed by a  $2 \times 2$  max-pooling layer; three fully connected layers with 1600, 120, and 64 units, respectively; and a 10-unit softmax output layer. Each convolution or fully connected layer is activated by the ReLU function. The CNN possesses 307842 parameters and our proposed FL approach only share the first 4 layers in the training process, which has 99.7% of the total number of model parameters. For both MLP and CNN, the learning rate  $\eta_u$  and  $\eta_v$  are set to 0.05, a momentum of 0.9 is adopted, the number of local iterations is set to 5, each parameter is quantitated as 16 bits, and cross entropy is adopted as the loss function.

2) System setting: If not specified, the system parameters related to communication and computation are set as follows. We consider that  $K = 100$  devices are randomly distributed within a  $500\text{m} \times 500\text{m}$  single cell with total bandwidth  $B = 10$  MHz, and the PS is located in the cell's centre. The channel noise power spectral density  $N_0$  is set to  $-174$  dBm. For all devices in the system, we set their maximum transmit power and CPU frequency as  $f_{k,\max} = 1\text{GHz}$  and  $p_{k,\max} = 1\text{W}$ , respectively. According to the real measurements in [26], we set the energy coefficient  $\kappa = 5 \times 10^{-27}$ . Similar to [35], the channel gain is modeled as  $h_{k,t} = h_0 \rho_k(t) (d_0/d_k)^v$ , where  $h_0 = -30\text{dB}$  is the path loss constant;  $d_k$  is the distance between device  $k$  and the PS;  $d_0 = 1\text{m}$  is the reference distance;  $\rho_k(t) \sim \text{Exp}(1)$  is exponentially distributed with unit mean, which represents the small-scale fading channel power gain from the device  $k$  to the PS in round  $t$ ;  $d_0/d_k$  represents the large-scale path loss with  $v = 2$  being the path loss exponent. Besides, we set  $T_{\max} = 2\text{s}$  and  $\bar{E}_k = 0.1\text{J}$  for the MNIST dataset, and  $T_{\max} = 14\text{s}$  and  $\bar{E}_k = 2\text{J}$  for the CIFAR-10 dataset.

### B. Performance of Partial Model Parameters Aggregation

To verify the advantages of the proposed PMA-FL algorithm, we first compare its performance with two benchmarks. Note that, we do not consider the energy and bandwidth limitation in this subsection.

1) *FedRep* [21]: In each round, the selected devices sequentially train the feature extractor and predictor. After local training, the selected devices only upload their feature extractors for

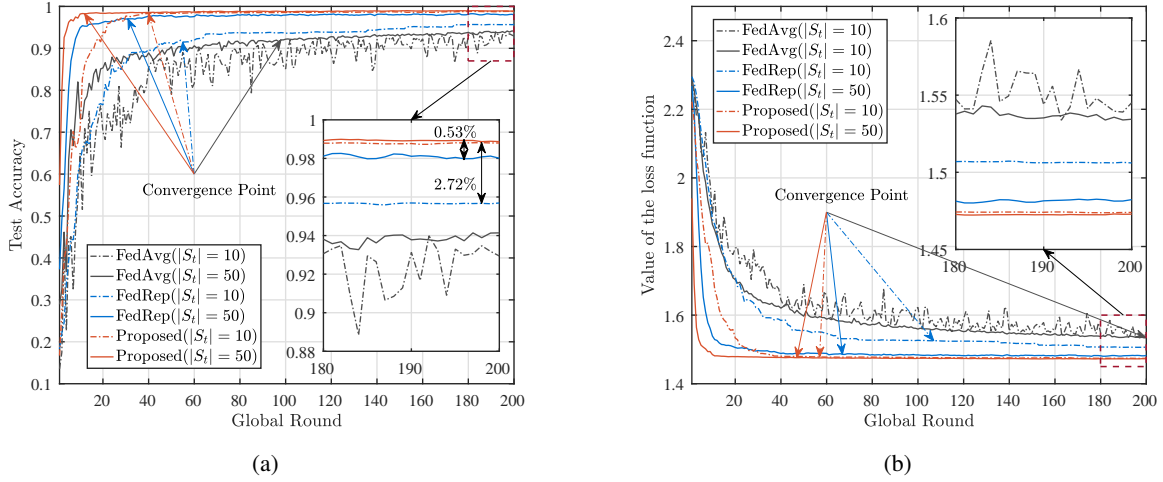


Fig. 3. Learning performance of the proposed partial aggregation approach and benchmarks on MNIST dataset: (a) test accuracy; (b) loss value.

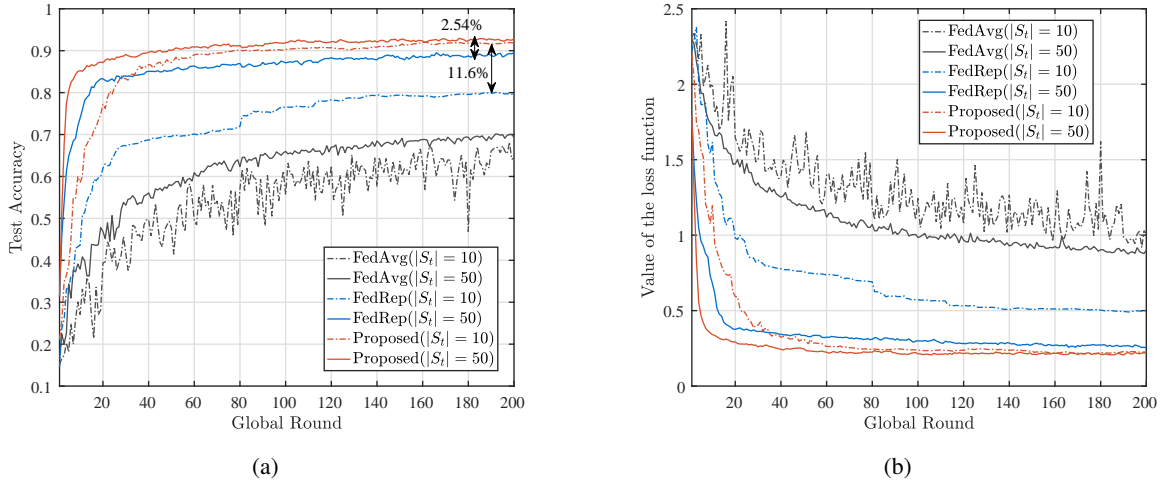


Fig. 4. Learning performance of the proposed partial aggregation approach and benchmarks on CIFAR-10 dataset: (a) test accuracy; (b) loss value.

aggregation. In fact, the local training and communication costs of FedRep is the same as the proposed approach. The difference is that the proposed approach simultaneously train feature extractor and predictor in every local iteration.

2) *FedAvg* [20]: In each round, the selected devices upload the entire model (including both feature extractor and predictor) to the PS for aggregation. Actually, FedAvg requires more computation and bandwidth resources than the proposed approach and FedRep.

Fig. 3 compares the performance of the proposed approach with two benchmarks on the MNIST dataset. It is observed that the proposed FL approach outperforms the benchmarks in terms of test accuracy and test loss. Specifically, the proposed approach boosts 2.72% when

$|S_t| = 10$  and 0.53% accuracy when  $|S_t| = 50$  compared with the state-of-art FedRep approach. Moreover, the proposed approach converges faster than the benchmarks. Note that the convergence point in 3(a) and 3(b) are defined as the first point that the variation of test accuracy and loss value is less than  $10^{-6}$ , respectively. Compared with the two benchmarks, the proposed approach is less sensitive to the fraction of participating devices in each round. After 40 global rounds, the proposed approach with 10 devices participating in each round can obtain a similar performance as 50 devices participating in each round. The device participating ratio only affects the convergence speed and almost without reducing the final accuracy. However, the benchmarks are sensitive for the fraction of participating devices in each round, especially the training process of FedAvg is unstable when the participating ratio of devices is small, like 10 devices.

Fig. 4 presents the performance of the proposed approach and two benchmarks on the CIFAR-10 datasets, drawing a similar conclusion with the experiments on the MNIST dataset. In particular, the proposed approach obtained a more distinct performance improvement on this more complicate dataset, boosting 11.6% and 2.54% accuracy than FedRep when  $|S_t| = 10$  and  $|S_t| = 50$ , respectively. Similarly, the learning process of FedAvg is unstable when a small fraction of devices participate in each round, i.e.,  $|S_t| = 10$ . These results indicate that the proposed approach with partial model aggregation is more robust, performing well in real datasets.

### C. Performance of the Proposed Energy-Efficient Device Scheduling Algorithm

In this subsection, we verify the effectiveness of the proposed dynamic device scheduling algorithm by comparing it with the following device scheduling schemes. For fairness, we use these benchmark schemes to schedule devices for the proposed FL approach instead of their original FedAvg approach.

1) *Random scheduling without energy limitation (RS-WEL)*: Devices do not have energy limitation while the bandwidth and delay constraints exist. In each round, RS-WEL uses the set expansion algorithm to schedule devices. Specifically, it incrementally adds devices (randomly selected from all devices without replacement) into the scheduling set until violating the bandwidth constraint. Then, the last scheduling set that satisfies bandwidth constraints is the true scheduling device set.

2) *OCEAN* [11]: The OCEAN is also a Lyapunov optimization-based device scheduling approach, in which the spectral bandwidth is orthogonally allocated to the scheduled devices for

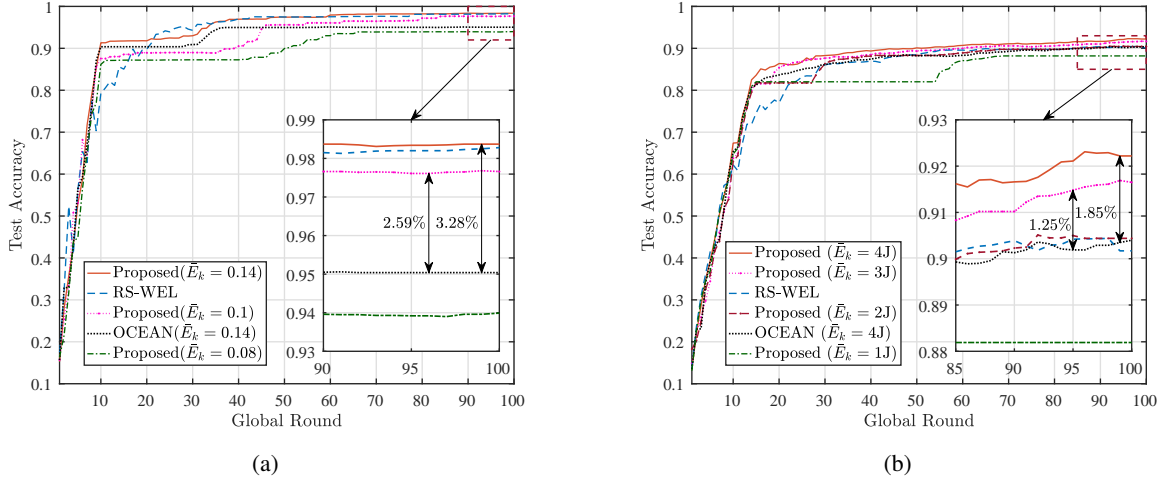


Fig. 5. Performance of the proposed algorithm and benchmarks under different energy budget  $\bar{E}_k$ : (a) on MNIST dataset; (b) on CIFAR-10 dataset.

global aggregation in each communication round.

Based on the MNIST dataset, Fig. 5(a) shows the effect of devices' energy budget on the training performance of the proposed dynamic device scheduling algorithm and two benchmarks. The results indicate that our proposed dynamic device scheduling algorithm outperforms the two benchmarks. Given the same energy budget, i.e.,  $\bar{E}_k = 0.14J$ , the proposed algorithm achieves 3.28% test accuracy improvement comparing with the state-of-art OCEAN algorithm. Moreover, the proposed algorithm is able to obtain better performance than the OCEAN algorithm under less energy budget. Specifically, the proposed algorithm with energy budget  $\bar{E}_k = 0.1J$  (71% of the energy budget of OCEAN) remains improving 2.59% accuracy compared to the OCEAN algorithm with energy budget  $\bar{E}_k = 0.14J$ . Compared with the RS-WEL scheme with unlimited energy budget, the proposed algorithm achieves a slight accuracy improvement when the energy budget is  $\bar{E}_k = 0.14J$ .

A similar evaluation is made on the CIFAR-10 dataset in Fig. 5(b). Given energy budget  $\bar{E}_k = 4J$  for both the proposed algorithm and the OCEAN algorithm, the proposed algorithm achieves around a 1.85% accuracy boosts for the OCEAN algorithm. Similarly, the proposed algorithm under 75% energy budget ( $\bar{E}_k = 3J$ ) outperforms the OCEAN algorithm with an energy budget  $\bar{E}_k = 4J$ , obtaining 1.25% accuracy gain. Additionally, the proposed algorithm with  $\bar{E}_k = 2J$  obtains a similar performance as the OCEAN algorithm with  $\bar{E}_k = 4J$  and the RS-WEL scheme. The performance gain mainly comes from the joint optimization for both computation and wireless resources. In our proposed algorithm, the participating devices can



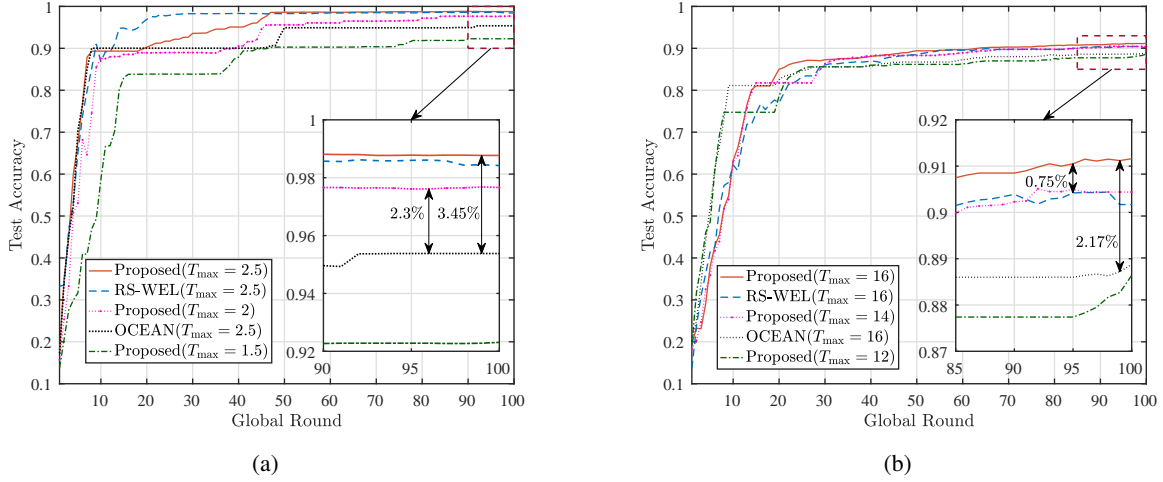


Fig. 6. Performance of the proposed algorithm and benchmarks under different delay constraint  $T_{\max}$ : (a) on MNIST dataset; (b) on CIFAR-10 dataset.

get a trade-off between computation and communication energy consumption, achieving the most energy-efficient learning process. Specifically, the devices with poor channel conditions can boost their CPU frequency for reducing computation time and thus reserve more time for wireless communications. In contrast, devices with good channel conditions can lower the CPU frequency to balance computation and communication energy consumption.

We compare our proposed device scheduling algorithm with the benchmarks under different latency constraints on MNIST dataset in Fig. 6(a). Clearly, as the latency constraint,  $T_{\max}$ , increases, the learning performance is improved. This is because a larger  $T_{\max}$  helps save the computation and communication energy and thus more data samples are able to scheduled in each round. Moreover, with the same latency constraints, i.e.,  $T_{\max} = 2.5$ s, the proposed algorithm boosts 3.45% test accuracy compared with the OCEAN algorithm. Using the RS-WEL as the baseline, the proposed algorithm obtains a minor accuracy gain. One interesting phenomenon is that the proposed algorithm outperforms the OCEAN algorithm with a stricter delay restriction. Specifically, given time budget  $T_{\max} = 2$ s for the proposed algorithm, it obtains 2.3% accuracy gain than the OCEAN algorithm with  $T_{\max} = 2.5$ s. In other words, the proposed algorithm is able to obtain a better accuracy with a 20% time budget reduction. Although the proposed algorithm with  $T_{\max} = 1.5$ s performs not good as the OCEAN algorithm with  $T_{\max} = 2.5$ s, the above results illustrate it has the ability to improve accuracy with a stringent delay.

Fig. 6(b) shows the impact of time budget on CIFAR-10 dataset, obtaining a similar results on the MNIST dataset. Specifically, the proposed algorithm boosts 2.17% test accuracy with

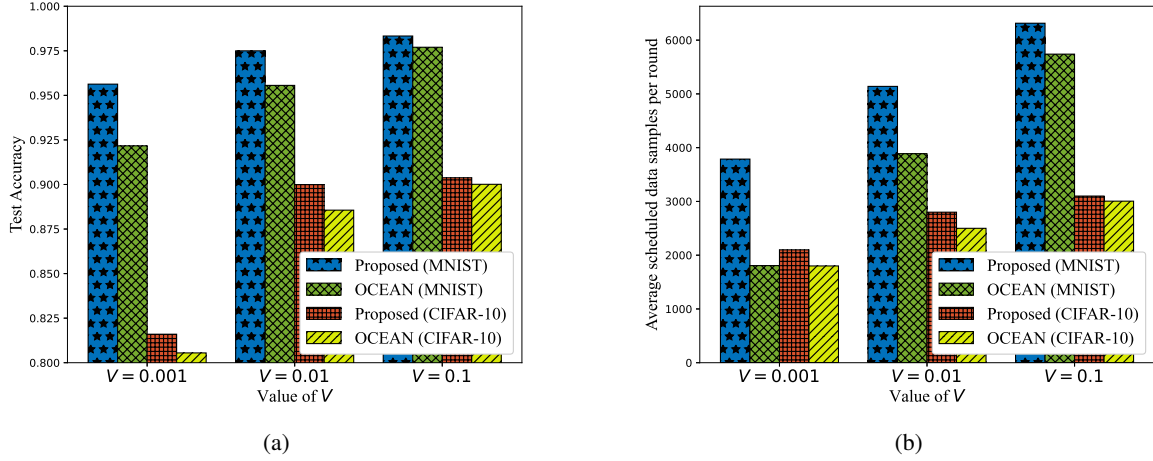


Fig. 7. Performance of the proposed algorithm and benchmarks under different weight parameter  $V$ : (a) test accuracy on MNIST and CIFAR-10 datasets; (b) average scheduled data samples per round.

the OCEAN algorithm under same delay restriction  $T_{\max} = 16s$ . Compared with the RS-WEL scheme, the proposed algorithm gains 0.75% performance improvement with  $T_{\max} = 16s$ , and obtains a similar performance with  $T_{\max} = 14s$ . Moreover, under a stringent delay requirement, i.e.,  $T_{\max} = 14s$ , the proposed algorithm achieves a better performance than the OCEAN algorithm with  $T_{\max} = 16s$ . That is, the proposed algorithm is able to get a better performance as the OCEAN algorithm with 12.5% time budget reduction. The underlying reason is that the joint optimization of computation and communication achieves lower energy consumption than solely considering the optimal communication. Even with less time budget, the balance between computation and communication can also lower the overall energy consumption, enabling more devices to participate in the FL training process in a sustainable way.

In Fig. 7, we verify that the adjustable weight parameter  $V$  is able to balance the training performance and energy consumption of devices. Fig. 7(b) shows that as  $V$  increases, devices consume energy in a more aggressive manner, resulting in scheduling more data samples, thus obtaining accuracy improvement. From Fig. 7(a), the experiments on the MNIST dataset indicate that the proposed algorithm achieves 3.46%, 1.94%, and 0.63% test accuracy improvement compared with the OCEAN algorithm under  $V = 0.001$ ,  $V = 0.01$ , and  $V = 0.1$ , in each one respectively. Interestingly, the proposed algorithm with  $V = 0.001$  obtains a similar performance with the OCEAN algorithm with  $V = 0.01$ . This further reveals that the proposed algorithm has the ability to obtain a similar performance as the OCEAN algorithm under a more rigid energy restriction. Similarly, on the CIFAR-10 dataset, the proposed algorithm boosts 1.05% and 1.23%

accuracy in terms of  $V = 0.001$  and  $V = 0.01$ , and obtains a slight accuracy improvement when  $V = 0.1$  compared with the OCEAN algorithm. Note that, if  $V$  is too large, the device scheduling algorithm would pay less attention for devices' energy consumption and try to schedule more devices. This may break the energy budget limitation for devices. Thus, the value of  $V$  should be judiciously adjusted to optimize the training performance while satisfying the long-term energy constraints.

## VI. CONCLUSION

In this work, we have proposed a novel PMA-FL algorithm, which only shares the feature extractor part of neural networks for global aggregation in the learning process while the predictor part of each device is localized for personalization. This design effectively improves the robustness and performance of the training process, overcoming the data heterogeneity across devices. The proposed PMA-FL offers an inspiring answer for the two motivation problems. For the first problem, PMA-FL optimizes the learning performance through achieving energy consumption balance between communication and computation for each device and energy consumption-bandwidth balance between devices. Compared with the considered benchmarks with the same energy and time budgets, PMA-FL obtained around 3% and 2% accuracy improvement on the MNIST and CIFAR-10 datasets, respectively. Moreover, PMA-FL is able to obtain slightly higher accuracy than the benchmarks with 29% energy or 20% time reduction on the MNIST; and 25% energy or 12.5% time reduction on the CIFAR-10. For the second problem, we have theoretically analyzed the convergence bound of PMA-FL with a general non-convex loss function setting. Experiments show that PMA-FL is able to boost 2.72% and 11.6% accuracy on MNIST and CIFAR-10 datasets compared to the state-of-art benchmarks, respectively.

## APPENDIX

### A. Proof of Lemma 1

Using  $L_u$ -smooth of  $F_k(\cdot, \mathbf{v}_k)$  and  $L_v$ -smooth of  $F(\mathbf{u}, \cdot)$ , we have:

$$F_k(\mathbf{u}_{t+1}, \mathbf{v}_{k,t+1}) - F_k(\mathbf{u}_t, \mathbf{v}_{k,t+1}) \leq \langle \nabla_{\mathbf{u}} F_k(\mathbf{u}_t, \mathbf{v}_{k,t+1}), \mathbf{u}_{t+1} - \mathbf{u}_t \rangle + \frac{L_u}{2} \|\mathbf{u}_{t+1} - \mathbf{u}_t\|^2, \quad (35)$$

and

$$F_k(\mathbf{u}_t, \mathbf{v}_{k,t+1}) - F_k(\mathbf{u}_t, \mathbf{v}_{k,t}) \leq \langle \nabla_{\mathbf{v}} F_k(\mathbf{u}_t, \mathbf{v}_{k,t}), \mathbf{v}_{k,t+1} - \mathbf{v}_{k,t} \rangle + \frac{L_v}{2} \|\mathbf{v}_{k,t+1} - \mathbf{v}_{k,t}\|^2. \quad (36)$$

Summarizing (35) and (36), we have

$$F_k(\mathbf{u}_{t+1}, \mathbf{v}_{k,t+1}) - F_k(\mathbf{u}_t, \mathbf{v}_{k,t}) \leq \langle \nabla_{\mathbf{v}} F_k(\mathbf{u}_t, \mathbf{v}_{k,t}), \mathbf{v}_{k,t+1} - \mathbf{v}_{k,t} \rangle + \frac{L_v}{2} \|\mathbf{v}_{k,t+1} - \mathbf{v}_{k,t}\|^2 \\ + \langle \nabla_{\mathbf{u}} F_k(\mathbf{u}_t, \mathbf{v}_{k,t+1}), \mathbf{u}_{t+1} - \mathbf{u}_t \rangle + \frac{L_u}{2} \|\mathbf{u}_{t+1} - \mathbf{u}_t\|^2. \quad (37)$$

We now bound the inner product term  $\langle \nabla_{\mathbf{u}} F_k(\mathbf{u}_t, \mathbf{v}_{k,t+1}), \mathbf{u}_{t+1} - \mathbf{u}_t \rangle$  as follows:

$$\langle \nabla_{\mathbf{u}} F_k(\mathbf{u}_t, \mathbf{v}_{k,t+1}), \mathbf{u}_{t+1} - \mathbf{u}_t \rangle \\ \stackrel{(a)}{=} \langle \nabla_{\mathbf{u}} F_k(\mathbf{u}_t, \mathbf{v}_{k,t}), \mathbf{u}_{t+1} - \mathbf{u}_t \rangle + \langle \nabla_{\mathbf{u}} F_k(\mathbf{u}_t, \mathbf{v}_{k,t+1}) - \nabla_{\mathbf{u}} F_k(\mathbf{u}_t, \mathbf{v}_{k,t}), \mathbf{u}_{t+1} - \mathbf{u}_t \rangle \\ \stackrel{(b)}{\leq} \langle \nabla_{\mathbf{u}} F_k(\mathbf{u}_t, \mathbf{v}_{k,t}), \mathbf{u}_{t+1} - \mathbf{u}_t \rangle + \|\nabla_{\mathbf{u}} F_k(\mathbf{u}_t, \mathbf{v}_{k,t+1}) - \nabla_{\mathbf{u}} F_k(\mathbf{u}_t, \mathbf{v}_{k,t})\| \|\mathbf{u}_{t+1} - \mathbf{u}_t\| \\ \stackrel{(c)}{\leq} \langle \nabla_{\mathbf{u}} F_k(\mathbf{u}_t, \mathbf{v}_{k,t}), \mathbf{u}_{t+1} - \mathbf{u}_t \rangle + L_{uv} \|\mathbf{v}_{k,t+1} - \mathbf{v}_{k,t}\| \|\mathbf{u}_{t+1} - \mathbf{u}_t\| \\ \stackrel{(d)}{\leq} \langle \nabla_{\mathbf{u}} F_k(\mathbf{u}_t, \mathbf{v}_{k,t}), \mathbf{u}_{t+1} - \mathbf{u}_t \rangle + \sqrt{\chi L_v} \|\mathbf{v}_{k,t+1} - \mathbf{v}_{k,t}\| \sqrt{\chi L_u} \|\mathbf{u}_{t+1} - \mathbf{u}_t\| \\ \stackrel{(e)}{\leq} \langle \nabla_{\mathbf{u}} F_k(\mathbf{u}_t, \mathbf{v}_{k,t}), \mathbf{u}_{t+1} - \mathbf{u}_t \rangle + \frac{1}{2} \chi L_v \|\mathbf{v}_{k,t+1} - \mathbf{v}_{k,t}\|^2 + \frac{1}{2} \chi L_u \|\mathbf{u}_{t+1} - \mathbf{u}_t\|^2, \quad (38)$$

where (a) is derived by adding and subtracting  $\nabla_{\mathbf{u}} F_k(\mathbf{u}_t, \mathbf{v}_{k,t})$ , (b) following the Cauchy-Schwarz inequality, (c) is due to Assumption 1, (d) is due to the definition of  $\chi$ , (e) comes from the triangle-inequality. Substituting (38) into (37), we have

$$F_k(\mathbf{u}_{t+1}, \mathbf{v}_{k,t+1}) - F_k(\mathbf{u}_t, \mathbf{v}_{k,t}) \leq \langle \nabla_{\mathbf{u}} F_k(\mathbf{u}_t, \mathbf{v}_{k,t}), \mathbf{u}_{t+1} - \mathbf{u}_t \rangle + \frac{1+\chi}{2} L_u \|\mathbf{u}_{t+1} - \mathbf{u}_t\|^2 \\ + \langle \nabla_{\mathbf{v}} F_k(\mathbf{u}_t, \mathbf{v}_{k,t}), \mathbf{v}_{k,t+1} - \mathbf{v}_{k,t} \rangle + \frac{1+\chi}{2} L_v \|\mathbf{v}_{k,t+1} - \mathbf{v}_{k,t}\|^2. \quad (39)$$

Substituting the above equation into the global loss function (2), the proof completes.

## B. Proof of Lemma 2

For ease of presentation, we define an auxiliary variable as follows:

$$\mathbf{o}_t = \nabla_{\mathbf{u}} F(\mathbf{u}_t, \mathbf{V}_t) - \frac{\sum_{k=1}^K \alpha_{k,t} D_k \nabla_{\mathbf{u}} F_k(\mathbf{u}_t, \mathbf{v}_{k,t})}{\sum_{k=1}^K \alpha_{k,t} D_k}. \quad (40)$$

Based on Lemma 1, we focus on bounding the two terms in the right-hand side (RHS) of (15).

For the first term in the RHS of (15), we have

$$\mathbb{E} \left[ \langle \nabla_{\mathbf{u}} F(\mathbf{u}_t, \mathbf{V}_t), \mathbf{u}_{t+1} - \mathbf{u}_t \rangle + \frac{1+\chi}{2} L_u \|\mathbf{u}_{t+1} - \mathbf{u}_t\|^2 \right] \\ = \mathbb{E} [\langle \nabla_{\mathbf{u}} F(\mathbf{u}_t, \mathbf{V}_t), -\eta_u (\nabla_{\mathbf{u}} F(\mathbf{u}_t, \mathbf{V}_t) - \mathbf{o}_t) \rangle] + \frac{1}{2} (\chi+1) L_u \mathbb{E} \|\eta_u (\nabla_{\mathbf{u}} F(\mathbf{u}_t, \mathbf{V}_t) - \mathbf{o}_t)\|^2 \\ = \left( \frac{(\chi+1)L_u}{2} \eta_u^2 - \eta_u \right) \mathbb{E} \|\nabla_{\mathbf{u}} F(\mathbf{u}_t, \mathbf{V}_t)\|^2 + \frac{(\chi+1)L_u}{2} \eta_u^2 \mathbb{E} \|\mathbf{o}_t\|^2 \\ + (\eta_u - (\chi+1)L_u \eta_u^2) \mathbb{E} [\langle \nabla_{\mathbf{u}} F(\mathbf{u}_t, \mathbf{V}_t), \mathbf{o}_t \rangle]$$

$$\stackrel{(a)}{\leq} -\frac{1}{2}\eta_u \mathbb{E} \|\nabla_{\mathbf{u}} F(\mathbf{u}_t, \mathbf{V}_t)\|^2 + \frac{1}{2}\eta_u \mathbb{E} \|\mathbf{o}_t\|^2, \quad (41)$$

where (a) is due to  $\eta_u \leq \frac{1}{(\chi+1)L_u}$  and the triangle-inequality. For the second term in the RHS of (15), we have

$$\begin{aligned} & \frac{1}{D} \sum_{k=1}^K D_k \left( \mathbb{E} [\langle \nabla_{\mathbf{v}} F_k(\mathbf{u}_t, \mathbf{v}_{k,t}), \mathbf{v}_{k,t+1} - \mathbf{v}_{k,t} \rangle] + \frac{1+\chi}{2} L_v \mathbb{E} \|\mathbf{v}_{k,t+1} - \mathbf{v}_{k,t}\|^2 \right) \\ &= \frac{1}{D} \sum_{k=1}^K D_k \mathbb{E} [\langle \nabla_{\mathbf{v}} F_k(\mathbf{u}_t, \mathbf{v}_{k,t}), -\alpha_{k,t} \eta_v \nabla_{\mathbf{v}} F_k(\mathbf{u}_t, \mathbf{v}_{k,t}) \rangle] \\ &+ \frac{1}{D} \sum_{k=1}^K D_k \frac{1}{2} (1+\chi) L_v \mathbb{E} \|\alpha_{k,t} \eta_v \nabla_{\mathbf{v}} F_k(\mathbf{u}_t, \mathbf{v}_{k,t})\|^2 \\ &\stackrel{(a)}{=} \sum_{k=1}^K \alpha_{k,t} \frac{D_k}{D} \left( \frac{(1+\chi)}{2} L_v \eta_v^2 - \eta_v \right) \mathbb{E} \|\nabla_{\mathbf{v}} F_k(\mathbf{u}_t, \mathbf{v}_{k,t})\|^2, \end{aligned} \quad (42)$$

where (a) follows the fact that  $\alpha_{k,t} \in \{0, 1\}$ , which induces  $\alpha_{k,t}^2 = \alpha_{k,t}$ . Substituting (41) and (42) into (15), we have

$$\begin{aligned} \mathbb{E} [F(\mathbf{u}_{t+1}, \mathbf{V}_{t+1}) - F(\mathbf{u}_t, \mathbf{V}_t)] &\leq -\frac{1}{2}\eta_u \mathbb{E} \|\nabla_{\mathbf{u}} F(\mathbf{u}_t, \mathbf{V}_t)\|^2 + \frac{1}{2}\eta_u \mathbb{E} \|\mathbf{o}_t\|^2 \\ &+ \frac{1}{D} \sum_{k=1}^K \alpha_{k,t} D_k \left( -\eta_v + \frac{1}{2}(1+\chi) L_v \eta_v^2 \right) \mathbb{E} \|\nabla_{\mathbf{v}} F_k(\mathbf{u}_t, \mathbf{v}_{k,t})\|^2. \end{aligned} \quad (43)$$

Next, we focus on bounding  $\|\mathbf{o}_t\|^2$ .

$$\begin{aligned} \mathbb{E} \|\mathbf{o}_t\|^2 &= \mathbb{E} \left\| \nabla_{\mathbf{u}} F(\mathbf{u}_t, \mathbf{V}_t) - \frac{\sum_{k=1}^K \alpha_{k,t} D_k \nabla_{\mathbf{u}} F_k(\mathbf{u}_t, \mathbf{v}_{k,t})}{\sum_{k=1}^K \alpha_{k,t} D_k} \right\|^2 \\ &= \mathbb{E} \left\| -\frac{(D - \sum_{k=1}^K \alpha_{k,t} D_k) \sum_{k=1}^K \alpha_{k,t} D_k \nabla_{\mathbf{u}} F_k(\mathbf{u}_t, \mathbf{v}_{k,t})}{D \sum_{k=1}^K \alpha_{k,t} D_k} + \frac{\sum_{k=1}^K (1 - \alpha_{k,t}) D_k \nabla_{\mathbf{u}} F_k(\mathbf{u}_t, \mathbf{v}_{k,t})}{D} \right\|^2 \\ &\leq \mathbb{E} \left( \frac{(D - \sum_{k=1}^K \alpha_{k,t} D_k) \sum_{k \in \mathcal{K}_{1,t}} D_k \|\nabla_{\mathbf{u}} F_k(\mathbf{u}_t, \mathbf{v}_{k,t})\|}{D \sum_{k=1}^K \alpha_{k,t} D_k} + \frac{\sum_{k \in \mathcal{K}_{2,t}} D_k \|\nabla_{\mathbf{u}} F_k(\mathbf{u}_t, \mathbf{v}_{k,t})\|}{D} \right)^2, \end{aligned} \quad (44)$$

where  $\mathcal{K}_{1,t} = \{\alpha_{k,t} = 1 \mid k \in \mathcal{K}\}$  is the set of devices who participating the training process in round  $t$ , and  $\mathcal{K}_{2,t} = \{\alpha_{k,t} = 0 \mid k \in \mathcal{K}\}$  represents the set of devices that have not been selected in round  $t$ . The inequality in (44) follows the triangle-inequality. By using Assumption 2, we have

$$\sum_{k \in \mathcal{K}_{1,t}} D_k \|\nabla_{\mathbf{u}} F_k(\mathbf{u}_t, \mathbf{v}_{k,t})\| \leq \sum_{k=1}^K \alpha_{k,t} D_k \sqrt{\delta^2 + \rho^2 \|\nabla_{\mathbf{u}} F(\mathbf{u}, \mathbf{V})\|^2}, \quad (45)$$

and

$$\sum_{k \in \mathcal{K}_{2,t}} D_k \|\nabla_{\mathbf{u}} F_k(\mathbf{u}_t, \mathbf{v}_{k,t})\| \leq (D - \sum_{k=1}^K \alpha_{k,t} D_k) \sqrt{\delta^2 + \rho^2 \|\nabla_{\mathbf{u}} F(\mathbf{u}, \mathbf{V})\|^2}. \quad (46)$$

Substituting (45) and (46) into (44), we have

$$\mathbb{E} \|\mathbf{o}_t\|^2 \leq \frac{4(D - \sum_{k=1}^K \alpha_{k,t} D_k)^2 (\delta^2 + \rho^2 \|\nabla_{\mathbf{u}} F(\mathbf{u}, \mathbf{V})\|^2)}{D^2}. \quad (47)$$

Now, by substituting (47) into (43) and let  $\eta_v \leq \frac{2}{(\chi+1)L_v}$ , the proof completes.

### C. Proof of Theorem 1

To prove Theorem 1, we first prove that  $\nabla_{\mathbf{u}} F(\mathbf{u}, \mathbf{V})$  is  $L_u$ -Lipschitz continuous with  $\mathbf{u}$ .

$$\begin{aligned} \|\nabla_{\mathbf{u}} F(\mathbf{u}, \mathbf{V}) - \nabla_{\mathbf{u}} F(\mathbf{u}', \mathbf{V})\| &= \left\| \nabla_{\mathbf{u}} \left( \frac{1}{D} \sum_{k=1}^K D_k F_k(\mathbf{u}, \mathbf{v}_k) \right) - \nabla_{\mathbf{u}} \left( \frac{1}{D} \sum_{k=1}^K D_k F_k(\mathbf{u}', \mathbf{v}_k) \right) \right\| \\ &= \frac{1}{D} \left\| \sum_{k=1}^K D_k \left( \nabla_{\mathbf{u}} F_k(\mathbf{u}, \mathbf{v}_k) - \nabla_{\mathbf{u}} F_k(\mathbf{u}', \mathbf{v}_k) \right) \right\| \\ &\stackrel{(a)}{\leq} \frac{1}{D} \sum_{k=1}^K D_k \left\| \left( \nabla_{\mathbf{u}} F_k(\mathbf{u}, \mathbf{v}_k) - \nabla_{\mathbf{u}} F_k(\mathbf{u}', \mathbf{v}_k) \right) \right\| \\ &\stackrel{(b)}{\leq} \frac{1}{D} \sum_{k=1}^K D_k L_u \|\mathbf{u} - \mathbf{u}'\| = L_u \|\mathbf{u} - \mathbf{u}'\|, \end{aligned} \quad (48)$$

where (a) follows Cauchy-Schwarz inequality, (b) is due to the  $L_u$ -Lipschitz continuity of  $\nabla_{\mathbf{u}} F_k(\mathbf{u}, \mathbf{v}_k)$  ( $\forall k \in \mathcal{K}$ ). Thus,  $\nabla_{\mathbf{u}} F(\mathbf{u}, \mathbf{V})$  is  $L_u$ -Lipschitz continuous with  $\mathbf{u}$ . According to Lemma 2, we add and subtract  $F(\mathbf{u}^*, \mathbf{V}^*)$  in the left-hand side of (16), and then rearrange it gives

$$\begin{aligned} \mathbb{E} [F(\mathbf{u}_{t+1}, \mathbf{V}_{t+1}) - F(\mathbf{u}^*, \mathbf{V}^*)] &\leq \mathbb{E} [F(\mathbf{u}_t, \mathbf{V}_t) - F(\mathbf{u}^*, \mathbf{V}^*)] + \frac{2\eta_u}{D^2} \left( D - \sum_{k=1}^K \alpha_{k,t} D_k \right)^2 \delta^2 \\ &\quad + \frac{1}{2} \eta_u \left( \frac{4}{D^2} \left( D - \sum_{k=1}^K \alpha_{k,t} D_k \right)^2 \rho^2 - 1 \right) \mathbb{E} \|\nabla_{\mathbf{u}} F(\mathbf{u}_t, \mathbf{V}_t)\|^2. \end{aligned} \quad (49)$$

By using the  $L_u$ -Lipschitz continuity of  $\nabla_{\mathbf{u}} F(\mathbf{u}, \mathbf{V})$  is  $L_u$ , we have

$$\|\nabla_{\mathbf{u}} F(\mathbf{u}, \mathbf{V})\|^2 \leq 2L_u \left( F(\mathbf{u}, \mathbf{V}) - F(\mathbf{u}^*, \mathbf{V}^*) \right). \quad (50)$$

Substituting (50) into (49), we have

$$\mathbb{E} [F(\mathbf{u}_{t+1}, \mathbf{V}_{t+1}) - F(\mathbf{u}^*, \mathbf{V}^*)] \leq A_t \mathbb{E} [F(\mathbf{u}_t, \mathbf{V}_t) - F(\mathbf{u}^*, \mathbf{V}^*)] + 2\eta_u \frac{\left( D - \sum_{k=1}^K \alpha_{k,t} D_k \right)^2 \delta^2}{D^2}, \quad (51)$$

where  $A_t = \left( 1 + \eta_u L_u \left( \frac{4}{D^2} \left( D - \sum_{k=1}^K \alpha_{k,t} D_k \right)^2 \rho^2 - 1 \right) \right)$ . By telescoping the above inequality, we complete the proof.

### D. Proof of Lemma 3

In problem  $\mathcal{P}_3$ , the communication time variable  $T_{k,t}^L$  ( $\forall k \in \mathcal{K}$ ) is continuous real number variable. The first-order derivatives of the objective function is

$$\frac{\partial E_{k,t}}{\partial T_{k,t}^L} = -2\frac{\kappa\tau^3 D_k^3 C_k^3}{(T_{k,t}^L)^3} + \frac{\theta_{k,t} B N_0}{h_{k,t}} \left( \left( \frac{Q \ln 2}{\theta_{k,t} B (T_{\max} - T_{k,t}^L)} - 1 \right) 2^{\frac{Q}{\theta_{k,t} B (T_{\max} - T_{k,t}^L)}} + 1 \right). \quad (52)$$

Furthermore, if  $k \neq h$ , we have  $\frac{\partial^2 E_{k,t}}{\partial T_{k,t}^L \partial T_{h,t}^L} = 0$ . When  $k = h$ , the second-order derivatives is given by

$$\frac{\partial^2 E_{k,t}}{\partial (T_{k,t}^L)^2} = 6\frac{\kappa\tau^3 D_k^3 C_k^3}{(T_{k,t}^L)^4} + \frac{Q^2 N_0 (\ln 2)^2 2^{\frac{Q}{\theta_{k,t} B (T_{\max} - T_{k,t}^L)}}}{\theta_{k,t} B h_{k,t} (T_{\max} - T_{k,t}^L)^3}. \quad (53)$$

It is straightforward to see that  $\frac{\partial^2 E_{k,t}}{\partial (T_{k,t}^L)^2} \geq 0$ . Thus, the Hessian matrixes of  $E_{k,t}$  with respect to  $T_{k,t}^L$  is a diagonal matrix and the elements on the diagonal are all non-negative. Consequently, the Hessian matrix of  $E_{k,t}$  is semi-positive matrix and  $E_{k,t}$  is a convex function with respect to  $T_{k,t}^L$ . Moreover, the constraints in problem  $\mathcal{P}_3$  are all linear with respect to  $T_{k,t}^L$ . This implements that problem  $\mathcal{P}_3$  is convex. By using Karush-Kuhn-Tucker condition, we have the optimal solution satisfy  $\frac{\partial E_{k,t}}{\partial T_{k,t}^L} = 0$ . In fact,  $\frac{\partial E_{k,t}}{\partial T_{k,t}^L} = 0$  is equivalent to  $\frac{\partial E_{k,t}^L}{\partial T_{k,t}^L} = \frac{\partial E_{k,t}^U}{\partial T_{k,t}^U}$ .

## REFERENCES

- [1] Z. Chen, W. Yi, A. Nallanathan, and G. Y. Li, "Is partial model aggregation energy-efficient for federated learning enabled wireless networks?" submitted to IEEE Global Communications Conference (GLOBECOM 2022).
- [2] P. Kairouz, H. B. McMahan, B. Avent, A. Bellet, M. Bennis, A. N. Bhagoji, K. Bonawitz, Z. Charles, G. Cormode, R. Cummings, *et al.*, "Advances and open problems in federated learning," *arXiv preprint arXiv:1912.04977*, 2019.
- [3] H. Ye, L. Liang, and G. Y. Li, "Decentralized federated learning with unreliable communications," *IEEE J. Sel. Topics in Signal Processing*, pp. 1–1, 2022.
- [4] Z. Yang, M. Chen, K. Wong, H. Poor, and S. Cui, "Federated learning for 6G: Applications, challenges, and opportunities," *arXiv preprint arXiv:2101.01338*, 2021.
- [5] Z. Qin, G. Y. Li, and H. Ye, "Federated learning and wireless communications," *IEEE Wireless Commun.*, vol. 28, no. 5, pp. 134–140, 2021.
- [6] Y. Deng, M. M. Kamani, and M. Mahdavi, "Adaptive personalized federated learning," *arXiv preprint arXiv:2003.13461*, 2020.
- [7] Q. Zeng, Y. Du, K. Huang, and K. K. Leung, "Energy-efficient resource management for federated edge learning with CPU-GPU heterogeneous computing," *IEEE Trans. Wireless Commun.*, vol. 20, no. 12, pp. 7947–7962, 2021.
- [8] B. Luo, X. Li, S. Wang, J. Huang, and L. Tassiulas, "Cost-effective federated learning in mobile edge networks," *IEEE J. Sel. Areas Commun.*, vol. 39, no. 12, pp. 3606–3621, 2021.
- [9] K. Guo, Z. Chen, H. H. Yang, and T. Q. Quek, "Dynamic scheduling for heterogeneous federated learning in private 5G edge networks," *IEEE J. Sel. Topics in Signal Processing*, pp. 1–1, 2021.
- [10] W. Shi, S. Zhou, Z. Niu, M. Jiang, and L. Geng, "Joint device scheduling and resource allocation for latency constrained wireless federated learning," *IEEE Trans. Wireless Commun.*, vol. 20, no. 1, pp. 453–467, 2021.
- [11] J. Xu and H. Wang, "Client selection and bandwidth allocation in wireless federated learning networks: A long-term perspective," *IEEE Trans. Wireless Commun.*, vol. 20, no. 2, pp. 1188–1200, 2021.
- [12] Y. Sun, S. Zhou, Z. Niu, and D. Gündüz, "Dynamic scheduling for over-the-air federated edge learning with energy constraints," *IEEE J. Sel. Areas Commun.*, vol. 40, no. 1, pp. 227–242, 2022.

- [13] J. Ren, Y. He, D. Wen, G. Yu, K. Huang, and D. Guo, "Scheduling for cellular federated edge learning with importance and channel awareness," *IEEE Trans. Wireless Commun.*, vol. 19, no. 11, pp. 7690–7703, 2020.
- [14] M. Chen, Z. Yang, W. Saad, C. Yin, H. V. Poor, and S. Cui, "A joint learning and communications framework for federated learning over wireless networks," *IEEE Trans. Wireless Commun.*, vol. 20, no. 1, pp. 269–283, 2021.
- [15] S. Zhou and G. Y. Li, "Communication-efficient ADMM-based federated learning," *arXiv preprint arXiv:2110.15318*, 2021.
- [16] V. Smith, C.-K. Chiang, M. Sanjabi, and A. S. Talwalkar, "Federated multi-task learning," in *Proc. Neural Information Processing Systems (NeurIPS)*, 2017.
- [17] Y. Jiang, J. Konečný, K. Rush, and S. Kannan, "Improving federated learning personalization via model agnostic meta learning," *arXiv preprint arXiv:1909.12488*, 2019.
- [18] T. Li, A. K. Sahu, M. Zaheer, M. Sanjabi, A. Talwalkar, and V. Smith, "Federated optimization in heterogeneous networks," *Proceedings of Machine Learning and Systems*, vol. 2, pp. 429–450, 2020.
- [19] D. Li and J. Wang, "Fedmd: Heterogenous federated learning via model distillation," *arXiv preprint arXiv:1910.03581*, 2019.
- [20] B. McMahan, E. Moore, D. Ramage, S. Hampson, and B. A. y. Arcas, "Communication-Efficient Learning of Deep Networks from Decentralized Data," in *Proc. Artificial Intelligence and Statistics (AISTATS)*, 20–22, Apr. 2017.
- [21] L. Collins, H. Hassani, A. Mokhtari, and S. Shakkottai, "Exploiting shared representations for personalized federated learning," in *Proc. International Conference on Machine Learning (ICML)*, 18–24 Jul 2021.
- [22] Y. Bengio, A. Courville, and P. Vincent, "Representation learning: A review and new perspectives," *IEEE Trans. pattern analysis and machine intelligence*, vol. 35, no. 8, pp. 1798–1828, 2013.
- [23] Y. LeCun, Y. Bengio, and G. Hinton, "Deep learning," *nature*, vol. 521, no. 7553, pp. 436–444, 2015.
- [24] S. P. Karimireddy, S. Kale, M. Mohri, S. Reddi, S. Stich, and A. T. Suresh, "SCAFFOLD: Stochastic controlled averaging for federated learning," in *Proc. International Conference on Machine Learning (ICML)*, 13–18, Jul. 2020.
- [25] P. Molchanov, S. Tyree, T. Karras, T. Aila, and J. Kautz, "Pruning convolutional neural networks for resource efficient inference," in *Proc. International Conference on Learning Representations (ICLR)*, April, 2017.
- [26] A. P. Miettinen and J. K. Nurminen, "Energy efficiency of mobile clients in cloud computing." *HotCloud*, vol. 10, pp. 1–7, 2010.
- [27] C. You, K. Huang, H. Chae, and B.-H. Kim, "Energy-efficient resource allocation for mobile-edge computation offloading," *IEEE Trans. Wireless Commun.*, vol. 16, no. 3, pp. 1397–1411, 2017.
- [28] C. Anil, J. Lucas, and R. Grosse, "Sorting out Lipschitz function approximation," in *Proc. International Conference on Machine Learning (ICML)*, 09–15 Jun 2019.
- [29] E. Abbasnejad, J. Shi, and A. van den Hengel, "Deep Lipschitz networks and dudley GANs," 2018. [Online]. Available: <https://openreview.net/forum?id=rkw-jlb0W>
- [30] A. Virmaux and K. Scaman, "Lipschitz regularity of deep neural networks: analysis and efficient estimation," in *Proc. Neural Information Processing Systems (NeurIPS)*, 2018.
- [31] H. Sifaou and G. Y. Li, "Robust federated learning via over-the-air computation," *arXiv preprint arXiv:2111.01221*, 2021.
- [32] M. J. Neely, "Stochastic network optimization with application to communication and queueing systems," *Synthesis Lectures on Communication Networks*, vol. 3, no. 1, pp. 1–211, 2010.
- [33] S. Boyd, S. P. Boyd, and L. Vandenberghe, *Convex optimization*. Cambridge university press, 2004.
- [34] I. Waldspurger, A. d'Aspremont, and S. Mallat, "Phase recovery, maxcut and complex semidefinite programming," *Mathematical Programming*, vol. 149, no. 1, pp. 47–81, 2015.
- [35] X. Deng, J. Li, C. Ma, K. Wei, L. Shi, M. Ding, W. Chen, and H. V. Poor, "On dynamic resource allocation for blockchain assisted federated learning over wireless channels," *arXiv preprint arXiv:2105.14708*, 2021.